Advances in Applied Energy 3 (2021) 100032

Contents lists available at ScienceDirect

Advances in Applied Energy

journal homepage: www.elsevier.com/locate/adapen

Optimal hydrogen production in a wind-dominated zero-emission energy system

Lukas Weimann[a], Paolo Gabrielli[b], Annika Boldrini[a], Gert Jan Kramer[a], Matteo Gazzani[a,*]

[a] Copernicus Institute of Sustainable Development, Utrecht University, Utrecht 3584 CS, the Netherlands
[b] Institute of Energy and Process Engineering, ETH Zurich, Zurich 8092, Switzerland

ARTICLE INFO

Keywords:
Hydrogen economy
Power to hydrogen
Zero emission
MILP optimization
Energy system model

ABSTRACT

The role of hydrogen in future energy systems is widely acknowledged: from fuel for difficult-to-decarbonize applications, to feedstock for chemicals synthesis, to energy storage for high penetration of undispatchable renewable electricity. While several literature studies investigate such energy systems, the details of how electrolysers and renewable technologies optimally behave and interact remain an open question. With this work, we study the interplay between (i) renewable electricity generation through wind and solar, (ii) electricity storage in batteries, (iii) electricity storage via Power-to-H_2, and (iv) hydrogen commodity demand. We do so by designing a cost-optimal zero-emission energy system and use the Netherlands as a case study in a mixed integer linear model with hourly resolution for a time horizon of one year. To account for the significant role of wind, we also provide an elaborate approach to model broad portfolios of wind turbines. The results show that if electrolyzers can operate flexibly, batteries and power-to-H_2-to-power are complementary, with the latter using renewable power peaks and the former using lower renewable power outputs. If the operating modes of the power-to-H_2-to-power system are limited - artificially or technically - the competitive advantage over batteries decreases. The preference of electrolyzers for power peaks also leads to an increase in renewable energy utilization for increased levels of operation flexibility, highlighting the importance of capturing this feature both from a technical and a modeling perspective. When adding a commodity hydrogen demand, the amount of hydrogen converted to electricity decreases, hence decreasing its role as electricity storage medium.

1. Introduction

Limiting global warming to 1.5 °C, which is projected to significantly reduce the risk of climate change, requires global CO_2 emissions to be net-zero by 2050 [1]. This calls for an unprecedented transformation of all sectors associated with greenhouse gas emissions (GHGs), e.g. the power sector, agriculture, transportation, or industry. While technical solutions to effectively decarbonize local systems exist, the scale at which they must be deployed remains a major challenge. To name just a few critical aspects: the switch to solar- and wind-based electricity generation at a national and international level causes spatial and temporal supply-demand mismatch that needs to be balanced; a CO_2-neutral transportation sector requires new infrastructure and full replacement of fossil-driven internal combustion engines; and some key parts of the industrial sector would require a complete process redesign to avoid direct and indirect emissions. Clearly, multiple actions ranging from policy instruments to technical solutions are required to enable a timely transition to a CO_2-neutral society. In this framework, one important contribution is switching to a hydrogen economy. Although it is subject to discussion how and to what extent this should be realized, there is little doubt that hydrogen will play a key role in the future of many sectors [2].

Several studies on integrating hydrogen into energy systems can be found in open literature. We can recognize four main clusters: (i) High level studies focused on the whole energy system, typically with limited technical details, (ii) sector-specific studies, e.g. H_2 for industry, heating, or power market balancing, (iii) technical studies focused on a specific technology solution, e.g. wind turbines with electrolyzers or H_2 with CCS, and (iv) studies focused on the end-use of H_2 applications. We highlight and discuss a few important contributions from those clusters in the following lines.

Strachan et al.[3] investigated the role of hydrogen in the UK energy system with a strong focus on infrastructure. Endo et al.[4], Dodds et al.[5], Ball et al.[6], and Contreras et al.[7] studied the decarbonization of the transportation sector (especially road transport) for Japan, the UK, Germany, and the region of Madrid, Spain, respectively. They all found a significant role for H_2 fuel cell vehicles. Capros et al.[8,9] and Sgobbi et al.[10] analyzed more comprehensive decarbonization pathways for the EU, i.e. a broader set of technologies, energy carriers, and

* Corresponding author.
E-mail address: m.gazzani@uu.nl (M. Gazzani).

https://doi.org/10.1016/j.adapen.2021.100032
Received 26 April 2021; Received in revised form 30 April 2021; Accepted 30 April 2021
Available online 6 May 2021

Nomenclature

Acronyms

BoP	balance of plant
CCS	carbon capture and storage/sequestration
ENTSO-E	European network of transmission system operators for electricity
GHG	greenhouse gas emissions
KNMI	Dutch meteorology institute
LCOE	levelized cost of electricity
MES	multi-energy system
MILP	mixed integer linear programming
NGCC	natural gas combined cycle
O&M	operation and maintenance
PEMEC	polymer electrolyte membrane electrolyzer
PEMFC	polymer electrolyte membrane fuel cell
PtH_2	power-to-hydrogen
PV	photovoltaic panels
WT	wind turbines

Indices

i	technology
k	energy carrier
n	node
t	time

Sets

$\mathbb{N}$	natural numbers including zero
$\mathbb{R}$	real numbers
$\mathcal{M}$	set of all technologies
$\mathcal{N}$	set of all nodes
$\mathcal{T}$	hourly time horizon

Variables

$\mathbf{A}$	constraint matrix for continuous variables
$\mathbf{B}$	constraint matrix for binary variables
$\mathbf{b}$	constant term vector of MILP
$\mathbf{C}$	constraint matrix for integer variables
$\hat{\mathbf{c}}$	parameters of wind turbine cluster centroid
$\mathbf{d}$	cost vector for continuous variables
$\mathbf{e}$	cost vector for binary variables
$\mathbf{f}$	cost vector for integer variables
$\mathbf{x}$	continuous variable vector
$\hat{\mathbf{x}}$	parameters of wind turbine
$\mathbf{y}$	binary variable vector
$\mathbf{z}$	integer variable vector
D	distance between nodes
c	present value investment cost
c^{inv}	installed cost/total cost
D	water depth
d	distance to coast
E	energy content
e	emission factor
E^{in}	energy input
E^{out}	energy output
F	fuel input
f	fraction of installation cost over total cost
F^{max}	maximum fuel input
F^{min}	minimum fuel input
g	influence of ambient temperature
h	hub height for wind turbines
L	end-user demand
L^{SDC}	self-discharge loss
N	number of installed wind turbines
N^{c}	number of curtailed wind turbines
N^{max}	maximum number of wind turbines
P	output power
p	price
P^{max}	maximum power output for given weather conditions
P^{r}	rated power for wind turbines
r	spacing radius for wind turbines
r^*	discount rate
S	installed size
S^{max}	maximum size
S^{min}	minimum size
SF	scaling factor for wind turbines
T^{amb}	ambient temperature
U	energy import
u	average distance between individuals between neighboring clusters
v	wind speed
v^{in}	cut-in wind speed for wind turbines
v^{out}	cut-out wind speed for wind turbines
v^{r}	rated wind speed for wind turbines
w	average distances between individuals within cluster
x	ON/OFF status
$\mathcal{A}$	area designated for wind turbines
$\mathcal{S}$	silhouette value of cluster
α	connectivity
χ	objective function
Δ	self-discharge coefficient
δ	euclidean distance
η^{in}	charging efficiency
η^{out}	discharging efficiency
λ	cost coefficient
μ	cost coefficient
Φ	weather conditions
Π	self-discharge coefficient
ψ	maintenance cost fraction
σ	Installation decision for a given technology, boolean
τ^*	Average time of electricity stored in batteries
τ^{in}	number of time intervals required to completely charge storage medium
τ^{out}	number of time intervals required to completely discharge storage medium
θ	set of performance parameters
ξ	energy flow

sectors, and also found hydrogen to be an enabler for decarbonization. Most of these studies point out the ability of hydrogen to balance the supply-demand mismatch for electricity via power-to-hydrogen systems (PtH_2) as an additional advantage. However, being beyond their respective scope, none of these studies provide enough temporal, geographical, or technological detail to fully investigate this effect. More recent studies [11,12] tried to bring a greater level of detail to such system studies by sophisticated multi-scale modeling approaches. However, they are technologically broad and do not investigate PtH_2 systems in detail.

On the other hand, studies investigating the details of PtH_2 systems exist but they usually stick to a relatively small scale. This is a result of the trade-off between scale, time horizon, technical details, and temporal resolution dominating the computational tractability. Marchenko et al.[13] optimized an integrated power system, consisting of photovoltaics (PV), wind turbines (WT), batteries, and a PtH_2 system, to supply 10 kW and 100 kW of electricity in the Lake Baikal region in Russia. Zhang et al.[14,15] and Kalinci et al.[16] investigated similar systems to supply the electricity demand of an island, the former providing great detail by including power flow equations and reliability considerations. Schnuelle et al.[17] tried to identify the best combination of wind turbines and electrolyzers by comparing different electrolyzers and

including dynamic operation and transient power profiles. Bødal et al. [18] pointed out the importance of flexibility for PtH_2 in the integrated electricity and hydrogen energy systems for Texas in 2050, while Welder et al. [19] studied the development of the H_2 network and storage in Germany for mobility and industry; both studies adopt temporally and geographically resolved optimizations but are focused mainly on the economic and environmental implications rather than technical details. In stark contrast, Ishaq et al.[20] and Khalid et al.[21] took a thermodynamic approach, providing exergy analyses of PV/WT/PtH_2 systems. More recently, the idea of creating a viable business case for PtH_2 by participating in the electricity and hydrogen markets gained some attraction. Koleva et al. [22] studied solar-driven hydrogen production with grid integration in California, Xiao et al. [23] studied a similar, but wind-driven, system in Denmark, Apostolou [24] studied a stand-alone PtH_2 system to provide grid balancing and hydrogen for transportation in Denmark, and Guinot et al. [25] studied a stand-alone system to provide grid balancing in France. The coherent conclusion of these studies was that electricity grid balancing does not constitute a viable business case today but has great potential for the future when electrolyzer and fuel cell costs drop. Naturally, such studies focus on the operator's point of view rather than the integrated system's optimum.

Another important application of H_2, albeit highly debated, is low-carbon heat provision, both at residential and industrial level. Here, the studies span a broad range from domestic heating with fuel cells in co-generation mode [26] up to utility plant scale with renewable energy sources [27]. The integration of and comparison with carbon-capture based routes is particularly important in this cost-sensitive sector as shown by Sunny et al.[28], who analyzed the regional transition of a heating sector from natural gas-based to hydrogen-based infrastructure in the UK, including H_2 and CO_2 infrastructure considerations.

No matter its application, hydrogen has to be supplied in a low-carbon manner to affect the carbon balance positively. The predominant technologies for hydrogen production are methane reforming, coal and biomass gasification, and electrolysis [2]. All of those technologies can provide low-carbon hydrogen; to do so, reforming and gasification processes require carbon capture and storage (CCS) technologies, while electrolysis requires carbon-free electricity - as for example provided by a 100% renewables-based energy system.[1] An analysis of low-carbon hydrogen supply chains, including a comparison of different production routes, is provided by Gabrielli et al.[29].

In this work we focus on renewables-based energy systems, which is attracting a lot of interest despite being a relatively new field [30]. In fact, Lund et al.[30] showed that there is still a lack of national and global studies, and that Power-to-X embedded in those systems need more research. This agrees with the findings of the literature review conducted in the course of the present work. In particular the application of PtH_2 in renewables-based energy systems on national or international scale was found to lack analyses where rigorous spatial-temporal optimization is coupled to adequate technical detail. Furthermore, the majority of studies listed so far pay little attention to storage of hydrogen, despite being a crucial part of the PtH_2 system. Especially if the PtH_2 system is intended to be used for balancing, i.e. the electrolyzer runs mainly on surplus electricity from renewables, the optimal sizing and operation of the hydrogen storage is an important and challenging issue that requires detailed technology models and adequate temporal resolution. Understanding the operation in particular requires a sufficient analysis time horizon to reveal seasonal effects.

Hence, the research objective of the present study is to create a deeper understanding of the role of H_2 as energy storage medium and of its carbon-free production in a renewable-based energy system, in particular wind-dominated as anticipated for the Netherlands (similar conditions may be found in other countries, e.g., UK and Denmark). Particular focus is put on (i) how such a system is optimally designed and operated in space and time, (ii) how constraining the operation of electrolyzers and fuel cells affects the system performance, and (iii) how a commodity hydrogen demand affects the system design and operation. Due to the aforementioned issues, an integral part of this research is to provide the methodological means that allow for such an analysis. Accordingly, the study goes beyond existing literature from different perspectives. On the one hand, it improves the understanding of the role of H_2 in a 100% renewable energy system on a national scale by adopting a sophisticated modeling tool that (a) has reliable, thermodynamics-based technology models which build upon, and extend, previous work on underground H_2 storage [31] and electrochemical technologies [32], (b) employs mathematical optimization considering both temporal and spatial discretization, allowing to co-optimize design and operation, and (c) couples the optimization of production and end-use technologies to infrastructure requirements and land availability. On the other hand, this study also provides new modeling techniques for considering large sets of preexisting and/or additionally built wind turbine models, which is a key design parameter for predominantly wind-based systems.

As framework for this study, we target the design of an energy system capable of supplying the whole Dutch electricity demand with maximum penetration of renewables, balanced by batteries and/or PtH_2 with hydrogen storage in salt caverns. It considers hourly resolution for a time horizon of one year and multiple nodes for geographical discretization. The spatially resolved system was modelled as a mixed integer linear program (MILP). To account for the volatility of wind, the model features a detailed approach to model onshore and offshore wind turbines, taking the vast set of currently existing turbines into consideration.

The paper is organized as follows. In Section 2 we present the system description, the scenarios simulated to answer the research questions, the general optimization framework, and the wind turbine modeling approach (and performance). In Section 3, we present the findings regarding the aforementioned research objectives. Finally, conclusions of the work and recommendations are provided in Section 4.

2. System description and optimization framework

2.1. System description and research design

In this study, an autarchic multi-energy system (MES) for the Netherlands comprising two energy vectors (electricity and hydrogen) was designed. Electricity can initially be provided by photovoltaic panels (PV), wind turbines (WT), and, as a back-up, by natural gas combined cycle (NGCC). The system can be balanced using batteries and/or a PtH_2 system, consisting of polymer electrolyte membrane electrolyzers and fuel cells (PEMEC and PEMFC), with hydrogen storage in salt caverns. In order to investigate both seasonal and daily balancing effects, a time horizon of one year with hourly resolution was used. As shown in Fig. 1, the system is also spatially aggregated into eight different zones (in the following referred to as nodes) of three types: offshore (three nodes), onshore (four nodes), and onshore with salt caverns (one node). Table 1 summarizes the available technologies for the different nodes. In agreement with the Dutch geological features, the salt caverns are exclusively located in the northern-most onshore node [33]. As shown in Fig. 2, wind turbines at offshore nodes produce electricity which is transported to the onshore nodes. At onshore nodes, electricity is produced by PV panels or wind turbines, stored in batteries, converted to H_2 through a PEMEC, or used to supply an end-user demand. Hydrogen can be stored in salt caverns, converted back to electricity through a PEMFC, or used to supply and end-user demand. The NGCC is not shown as part of the onshore node to emphasize that this technology is not specifically modeled. Instead, it is represented as an electricity import whose cost and carbon rate are the levelized cost of electricity (LCOE) and emission factor of an NGCC. This simplification is deemed justified since the

[1] It should be noted that 'renewable' does not necessarily imply 'carbon-free'. In the context of this paper, we limit the term 'renewables' to energy sources without direct CO_2 emissions, e.g. wind, solar, or hydro.

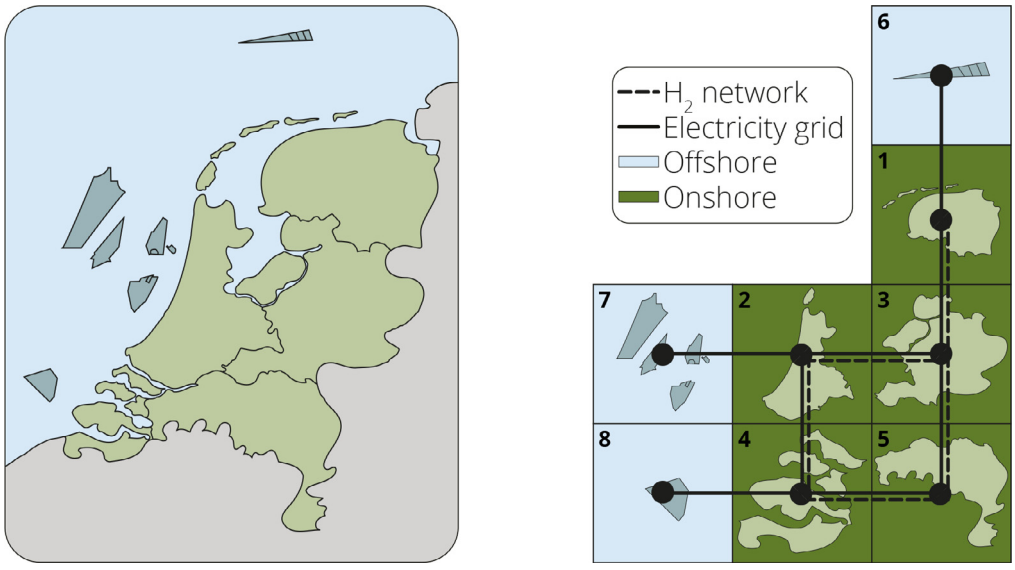

Fig. 1. Spatial aggregation of the Netherlands and potential network layout for hydrogen and electricity. The right-hand side is simplified to show the connectivity, i.e. the distances are not representative. The numbers in the top-left corners are the node-IDs.

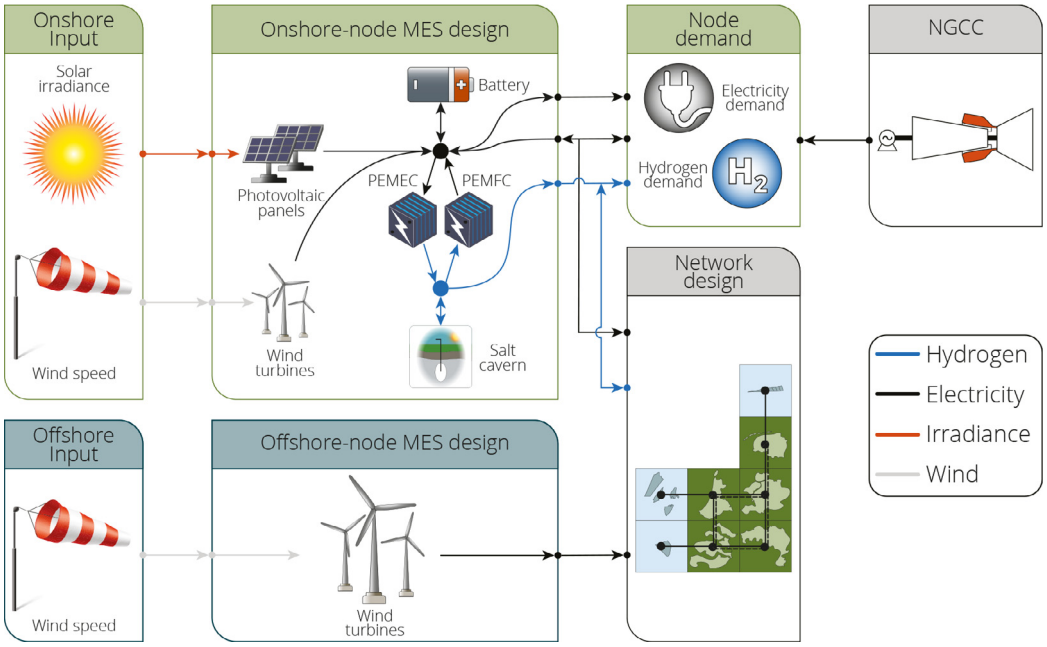

Fig. 2. Graphic summary of the MES design approach. Note that the hydrogen-cavern is only available in the northern-most onshore node (compare with Fig. 1 and Table 1).

Table 1
Summary of available technologies for the different types of nodes.

Node type	Conversion technologies	Balancing & storage technologies
offshore	WT	–
onshore	WT, PV, NGCC	PEMEC, PEMFC, battery
onshore w/salt cavern	WT, PV, NGCC	PEMEC, PEMFC, battery, salt cavern

main focus of this study is on zero-emission technologies. The reason for including NGCC at all is that the feasibility of a zero-emission design is not certain beforehand - requiring some sort of energy supply back-up - and likely not economically optimal. As shown in the results section, a zero-emission design proved to be feasible, but the NGCC is extensively used for cost-optimal designs with a non-zero constraint on emissions.

For the transport of both electricity and hydrogen between the nodes, a copper-plate approach was used as first modeling approach, i.e. the carriers are free to move between the nodes without constraints, and costs are neglected. As second step, we design both the hydrogen and electricity network. Discussion of this model relaxation is provided in Section 3.2. Finally, it is worth mentioning that a greenfield approach is used, except for wind turbines, for which all present installations are considered.

In order to address the research objectives raised in the introduction, three types of simulations have been conducted as shown in Fig. 3. First, the new wind turbine algorithm was assessed for its accuracy and

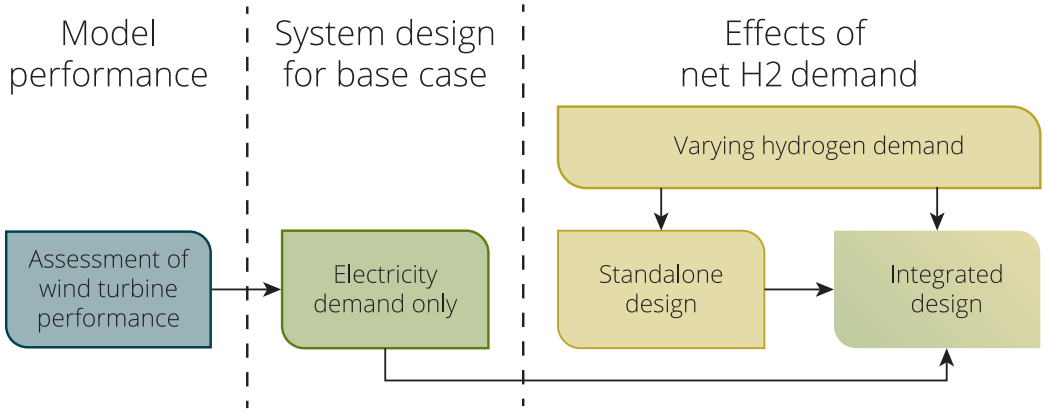

Fig. 3. Overview of the executed computational experiments.

computation time by analysing the model outcome as function of the key modeling parameters. We did this by optimally designing the full energy system shown in Fig. 2. Secondly, the base case, for which no hydrogen commodity demand is present, was analysed. Despite the absence of commodity hydrogen demand, PtH_2 technologies are available for storing electricity in the form of hydrogen. A Pareto optimization for emissions and cost was conducted, revealing the effect of CO_2 emission limits on the system design. For the two extreme designs, i.e. minimum cost and minimum emissions, a network was designed and analysed in a post-processing step. Finally, both integrated (electricity and hydrogen demand) and stand-alone systems (hydrogen demand only) were designed for different commodity hydrogen demands. The combination of these three types of analyses, namely base case design, stand-alone hydrogen design, and integrated design, allows to untangle the role of hydrogen in such systems. The problem is structured in an object-oriented script in Matlab R2018a [34], reshaped as matrix system using YALMIP toolbox [35] and solved with Gurobi v9 [36].

2.2. Optimization framework and methodology

The model in this work builds upon the framework developed by Gabrielli et al. [32,37], which optimizes the design and operation of MES to supply a fixed demand, utilizing the energy hub approach [38] via a mixed integer linear program (MILP). The general formulation of the MILP reads

$$\begin{aligned} \min_{\mathbf{x},\mathbf{y},\mathbf{z}} \quad & (\mathbf{d}'\mathbf{x} + \mathbf{e}'\mathbf{y} + \mathbf{f}'\mathbf{z}) \\ & \text{s.t.} \\ & \mathbf{A}\mathbf{x} + \mathbf{B}\mathbf{y} + \mathbf{C}\mathbf{z} = \mathbf{b} \\ & \mathbf{x} \geq 0 \in \mathbb{R}^{N_x}, \mathbf{y} \in \{0,1\}^{N_y}, \mathbf{z} \in \mathbb{N}^{N_z} \end{aligned} \tag{1}$$

where $\mathbf{d}$, $\mathbf{e}$, and $\mathbf{f}$ are the cost vectors with respect to continuous $\mathbf{x}$, binary $\mathbf{y}$, and integer variables $\mathbf{z}$. $\mathbf{A}$, $\mathbf{B}$, and $\mathbf{C}$ are their respective constraint matrices and $\mathbf{b}$ is the constant term of the constraints. N represents the dimensions of $\mathbf{x}$, $\mathbf{y}$, and $\mathbf{z}$ (indicated as subscript). More details can be found in Appendix A, while the full formulation is presented in Gabrielli et al. [37]. The model is geographically discretized and hourly resolved, where the time horizon depends on the input data provided. One year is considered in order to capture seasonal effects while keeping the computation time within reasonable bounds. To further reduce the computation time, 20 typical days were used to model the time horizon. However, this simplification was only applied to technologies assumed to operate in a seasonal manner, i.e. PEMEC, PEMFC, and hydrogen storage in salt caverns. All other conversion and storage technologies were modeled with the full time resolution of 8760 h (see M2 modeling strategy in Gabrielli et al. [37] for more details). Fig. 4 shows a summary of the framework in the physical and computational domains. In the following paragraphs, we qualitatively describe the key components of the model, which is reported as equations in Appendix A.

Input data. The model uses as input data (i) weather conditions (wind speed, solar irradiance, and ambient temperature), (ii) energy prices and (iii) carbon rates for energy flows crossing the system boundaries, and (iv) energy demands; all at hourly resolution for one year. This data is also spatially resolved as previously described. Another important set of input data are (v) technology cost and performance parameters, which are explained in Sections 2.3 and 2.4. In the present work, wind speed and solar irradiance data was obtained from the Dutch meteorology institute (KNMI) [39,40]. For each node, and because of the small area per node, the weather station that is closest to the node's center was selected. The total historic electricity load for the Netherlands with a time resolution of 15 min was obtained from the European network of transmission system operators for electricity (ENTSO-E) [41]. The data was averaged to obtain an hourly profile. In order to spatially distribute the demand, the annual demands of commercial properties [42] and domestic buildings [43,44] for each province were used to calculate a ratio-based distribution factor. As a result, the electricity demand profiles for the different nodes show the same qualitative trend but different magnitudes.

As opposed to the other technologies, the NGCC is not based on detailed models but implemented as electricity import that comes with an LCOE and emission factor representative of an NGCC, i.e. 40 EUR/MWh and 371 g/kWh, respectively.

Objective function. The (contrasting) objective functions to be minimized are the total annual costs and the total annual CO_2 emission. The total annual costs are composed of the annuitized investment cost, the operation and maintenance (O&M) as a percentage of the annuitized investment cost, and the costs of electricity import. Although the discount rate of 10% is the same for all technologies, the lifetime is specific for each technology, hence leading to different annuity factors. Production of carbon-containing energy carriers, e.g. extraction of natural gas or synthesis of methane, is not considered in this study, i.e. carbon sources can only enter the system as imports. Therefore, the emissions are calculated as the product of the amount of imported energy carrier and their respective carbon rate. Multi-objective optimization is realized via the ε-constraint method, resulting in Pareto-optimal designs.

Constraints. Four major classes of constraints are defined in this model: (i) performance of energy conversion technologies, (ii) performance of energy storage technologies, (iii) energy balances, and (iv) topographical constraints. For the former two, piecewise affine performance approximations are used whenever sensible. Key parameters for the specific technologies are reported in Sections 2.3 and 2.4. For details about the different technology models, the reader is referred to previous

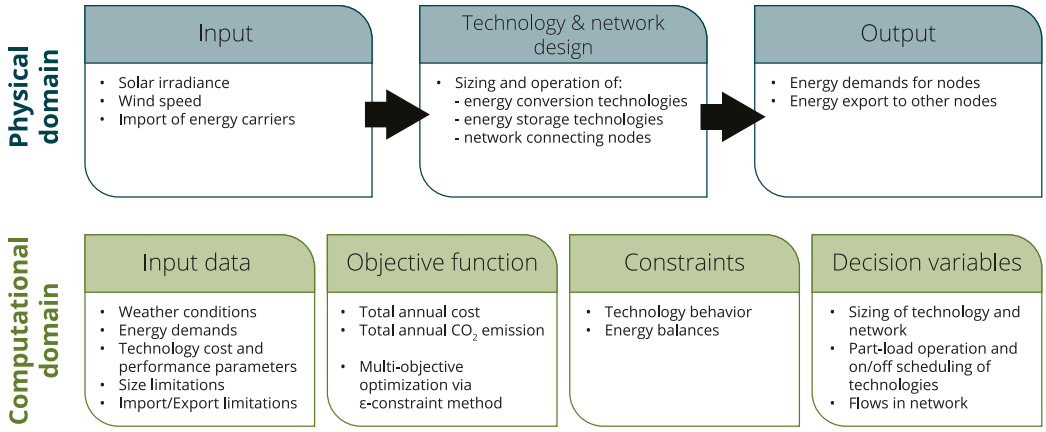

Fig. 4. Simplified representation of the physical information flow (top) and its translation into the MILP framework (bottom).

Table 2
Summary of economic and technical data of conversion and storage technologies. Operation and Maintenance (O&M) is given as percentage of the annuitized investment cost. The investment cost reported in this table is not annuitized.

Technology	Inv. cost [EUR/kW]	O&M [%]	Lifetime [y]	Avg efficiency [%]
PEMEC	345	5	20	53
PEMFC	241	8	20	51
PV	845	4	25	N.A.

Technology	Inv. cost [EUR/kWh]	O&M [%]	Lifetime [y]	Loss [%]		
				Charge	Discharge	Self-discharge
H_2 cavern	1	5	50	95	95	0
Battery	150	4	10	96	96	0.05

works using the same simulation tool [31,32,37,45–47]. The modeling of wind turbines, being a novel contribution of this paper, is treated separately in Section 2.4.

Constraints arising from topography are of interest for solar and wind power installations. Factors like suitable land or available rooftop space are translated into a maximum size value (see Eq. (21)), different for each node, to be processed by the model. For onshore wind installations, the available area was considered to be 15% of the total land [48,49]. For the potential of PV installations, the total Dutch rooftop area available is allocated over the five onshore nodes in proportion to the built-up area [50]. Finally, for offshore wind turbine installations, the area allocated by the Dutch government for 2030 was used [51]. The water depth and distance from shore, necessary to calculate the costs of offshore turbines, was retrieved from [52].

2.3. Energy conversion and storage technologies

The following paragraphs describe assumptions for cost and performance parameters related to the conversion and storage technologies specific for this study. For details about the technology models, references are given. Table 2 summarizes the key economic data and average efficiencies of the technologies discussed in this section. Technology costing for future energy systems - especially for technologies not currently deployed at scale - is always cumbersome and source of uncertainty. In this work, we decided to use costing information from transparent, detailed, and accessible literature sources, rather than manufacturer information. While realized values will somehow deviate from those used here, especially when accounting for specific market and geographic conditions, we argue that this does not substantially affect our findings (e.g. the system design), which are mainly driven by CO_2 emission minimization. The absolute cost results should be regarded as indicative of the order of magnitude and as an efficient metric to compare the different designs.

Electrolyzer and fuel cell. Because of the limited present production scale, rather than technological maturity, the current prices of electrolyzers and fuel cells are not representative of large-scale deployment. However, studies are available for large production scale. The National Renewable Energy Laboratory [53] reports electrolyzer prices at a scale of 50,000 units of 1 MW annually, based on a cost engineering approach. Whiston et al. [54] conducted an expert assessment resulting in an estimate for the fuel cell price at a scale of 500,000 units of 80 kW annually. However, neither of those studies paid special attention to the lifetime, in particular the difference in lifetime between the balance of plant (BoP) equipment and the cell stack.

For electrolyzers, starting from the detailed cost breakdown for stack and BoP repored in NREL [53] and assuming a lifetime of 20 years for the BoP equipment and five years for the stack, we discount the costs for the 3 replacements to get the present value. The total system cost can then be calculated according to Eq. (2).

$$c_{\text{system}} = c_{\text{BoP}} + c_{\text{stack}} \sum_{i=0}^{3} \frac{1}{(1+r^*)^{5i}} \tag{2}$$

where c is the present value investment cost and r^* is the discount rate.

For fuel cells, only the overall system cost are reported in Whiston et al. [54]. Assuming that electrolyzers and fuel cells have a similar ratio between BoP and stack costs, the system cost was split into stack and BoP cost and recalculated using Eq. (2). The model and performance parameters can be found in Gabrielli et al. [32]. A summary of the cost factors is provided in Table 3.

Table 3
Summary of cost factors for electrolyzers and fuel cells. All values in EUR/kW.

	c_{BoP}	c_{stack}	c_{system}	Reference
PEM Electrolyzer	146	89	345	[53]
PEM Fuel Cell	102	62	241	[53,54]

Photovoltaic panels. IRENA [55] reports installed costs for PV in 2019 to be 845 EUR/kW. A lifetime of 25 years is assumed based on common vendor warranties. The installation is limited to suited rooftop spaces, which constitute 200 km^2 in the Netherlands [56]. This rooftop space was allocated to the different onshore nodes in proportion to the built-up area [50]. The limitation to rooftops implies that PV and wind turbines do not compete for available land. The model and performance parameters can be found in Gabrielli et al. [37].

Hydrogen storage in salt caverns. According to a report from TNO [33], the Netherlands has a potential for 192.6 million m^3 of salt caverns. At a pressure of 100 bar and 50% cushion volume, this equates to roughly 100 PJ of hydrogen. Salt caverns totalling about 3 million m^3 already exist in the Netherlands and are currently used for natural gas storage [33]. The costs for hydrogen storage in salt caverns are, despite being a proven technology, hardly investigated. Argonne National Laboratory reported to the U.S. Department of Energy costs of 35-38 USD/kg_{H2} [57], or roughly 1 EUR/kWh_{H2}. This value includes the capital costs of auxiliary equipment like compressors. For the present study, it was assumed that the existing volume of 3 million m^3 comes free of investment cost (i.e. reusing both cavern and compression station) and expansion beyond this volume comes at the reported cost.

For the compression of hydrogen, an electrolyzer outlet pressure of 50 bar and a maximum cavern pressure of 102 bar was assumed [31]. As a conservative estimate, it was further assumed that hydrogen is always compressed to the maximum cavern pressure, independently of the actual cavern pressure. The pressure ratio of ~ 2 suggests the use of a single adiabatic compression stage, resulting in an electricity consumption for compression of 0.011 kWh_e/kWh_{H2}. The model and performance parameters not specified herein can be found in Gabrielli et al. [31].

Batteries. Based on data from Bloomberg NEF [58], the costs for Lithium-ion batteries were assumed to be 150 EUR/kWh. The model and performance parameters can be found in Gabrielli et al. [37].

2.4. Modeling of wind turbines

Wind energy is set to be a key renewable contributor in the power transition, and likely the largest in windy climate conditions as those found in e.g. the Netherlands, UK, or Denmark. As for the Dutch electricity mix, a significant amount of infrastructure already exists [59]. In order to account for these existing turbines as well as new turbines, we have developed a novel methodology for optimizing wind turbine portfolios in MILP. In the following, we elaborate on the general mathematical formulation of the wind turbine model, the treatment of existing turbines, and the simplifications required to keep the computation time within reasonable bounds. We conclude the section by evaluating the model performance and accuracy.

Mathematical description of wind turbines. The power output of a certain turbine can be described by its power curve, which is a function of the rated power, the wind speed at which the turbine starts producing electricity (cut-in wind speed), the wind speed at which the turbine reaches its rated power output (rated wind speed), and the wind speed at which the turbine has to be stopped (cut-out wind speed). Accordingly, the power curve is described by Eq. (3) [60].

$$P^{\max}(v) = \begin{cases} 0 & \text{if } v < v^{\text{in}} \\ P^{\text{r}} \frac{v^3 - \left(v^{\text{in}}\right)^3}{\left(v^{\text{r}}\right)^3 - \left(v^{\text{in}}\right)^3} & \text{if } v^{\text{in}} \le v < v^{\text{r}} \\ P^{\text{r}} & \text{if } v^{\text{r}} \le v < v^{\text{out}} \\ 0 & \text{if } v \ge v^{\text{out}} \end{cases} \tag{3}$$

where $P^{\max}$ is the maximum power output, P^{r} the rated power output (i.e. the maximum capacity), v the wind speed, and v^{in}, v^{r} and v^{out} the cut-in, rated and cut-out wind speed respectively. Although some turbines are engineered to withstand strong storms for a certain period of time, the cut-out wind speed for most turbines is 25 m/s [61], which is assumed here for all turbines, resulting in the power curve to be a function of three variables. In the Netherlands, wind speeds hardly reach this limit. In this study, we consider three types of onshore wind turbines for installation of new turbines, namely the Vestas V63 (1.5 MW), the Siemens SWT2.5 (2.5 MW), and the Vestas V120 (4.5 MW). For the installation of new offshore wind turbines, two types were selected; the Vestas V164 (9.5 MW), which is expected to be utilized in the Borssele V windpark [62], and the Siemens SWT6.0 (6.0 MW). The selected offshore turbines are notably larger than currently installed turbines, which is intended to reflect the trend towards bigger turbines. The technical parameters of the wind turbines are summarized in Table 4. On top of the five mentioned turbines, the existing Dutch wind turbines are considered as well.

The power output from wind turbines as imposed by the wind speed and described by eq. (3) is the upper limit for the net power output after curtailment $P_{i,t}$. Curtailment can be modelled in two ways: continuous or discrete. Continuous curtailment is implemented via an inequality and expressed as

$$P_{i,t} \le P_i^{\max}(v_t) N_i \tag{4}$$

where N is the number of installed turbines and i and t indicate the turbine type and time instant, respectively. Physically speaking, this formulation says that each turbine can produce any power output up to its maximum determined by the wind speed. Opposed to this, discrete curtailment (Eq. (5)) assumes that a turbine is either shut off or operates according to its power curve. This requires the introduction of a new integer variable, namely the number of curtailed turbines N^{c}.

$$P_{i,t} = (N_i - N_{i,t}^{\text{c}}) P_i^{\max}(v_t) \tag{5}$$

While the two methods converge for large values of N, outcomes can differ significantly for low values. The methods' effects on the system design and computation time have been investigated and are discussed below.

The number of installed turbines is limited by a maximum value $N^{\max}$ as well as by the available area. While $N^{\max}$ is defined for each turbine type, all types compete for the same area (Eqs. (6) and (7))

$$N_i \le N_i^{\max} \tag{6}$$

$$\sum_i N_i \pi r_i^2 \le \mathcal{A} \tag{7}$$

where $\mathcal{A}$ is the area designated for wind turbines and r the spacing radius for each wind turbine, i.e. two wind turbines have a minimum spacing of $2r$. This value is not to be mistaken with the rotor diameter. An average spacing radius for all turbine types of 400 m was assumed which is in agreement with existing wind farms [65,66], the often referred to rule of thumb of a spacing of 3–10 rotor diameters applied to a broad set of turbines [67], and also with real values presented in NREL [68]. For spatially resolved models like in this work, the number of turbines N_i, the designated area $\mathcal{A}$, and the wind speed v_t are defined for each node separately.

The wind speed at hub height was calculated using the 1/7th power law (Eq. (8)) [60,67]

$$v(h) = v(h_0) \left(\frac{h}{h_0} \right)^{1/7} \tag{8}$$

Table 4
Summary of wind turbines used in this study.

Acronym	Model	Domain	P^r [kW]	v^{in} [m/s]	v^r [m/s]	Reference
WT-1.5	Vestas V63	onshore	1500	4	16	[63]
WT-2.5	Siemens SWT2.5	onshore	2500	3	12	[63]
WT-4.5	Vestas V120	onshore	4500	4	12	[63]
WT-6.0	Siemens SWT6.0	offshore	6000	3	12	[63]
WT-9.5	Vestas V164	offshore	9500	3	13	[64]

where h is the hub height and h_0 the reference height. Assuming that the hub height of most future turbines falls into the range of 100 - 150 m [69], an average hub height h_{avg} to minimize the error in wind speed in that range was calculated according to

$$\min_{h_{avg}} \sum_{i=100}^{150} \left| v(i) - v(h_{avg}) \right| \tag{9}$$

The found value of $h_{avg} = 123$m was used for all turbines.

Modeling of diverse wind turbine portfolios. As the installed capacity of wind turbine grows, correct modeling of existing wind turbine farms is becoming more and more important. Not only does this allow for computing the power and energy output but also for identification of those sites that need to be replaced by newer turbines. The amount, rated capacity, and location of currently installed wind turbines in the Netherlands are publicly available [70]. However, the model described requires cut-in and rated wind speed on top of the rated power. To estimate these parameters, a database of commercial wind turbines, consisting of (i) manufacturer, (ii) cut-in wind speed, (iii) rated wind speed, and (iv) rated power, was created. Via arithmetic means and linear interpolation and extrapolation, the characteristics of the power curve can then be retrieved for a given rated power value and manufacturer. The so-gained information about existing wind turbines contains 121 different turbines (36 if the location is not treated as distinguishing parameter), of which a lot are very similar. Hence, the data set was clustered for three power curve characteristics using the k-means algorithm [71,72], which minimizes the sum of point-to-centroid distances. It is important to keep in mind that the centroids are not picked from the set of observations, i.e. they are not necessarily a turbine from the data set (see [73] for further information). This is important since the average performance of the clusters should be represented rather than a certain design parameter. Picking a turbine from the data set, as done for instance by the k-medoids algorithm, would divert from this purpose. The three dimensions (rated power, cut-in, and rated wind speed) were weighted equally by normalizing them and the squared euclidean distance δ was used as a distance metric

$$\delta(\hat{\mathbf{x}}, \hat{\mathbf{c}}) = (\hat{\mathbf{x}} - \hat{\mathbf{c}})(\hat{\mathbf{x}} - \hat{\mathbf{c}})' \tag{10}$$

where $\hat{\mathbf{x}}$ and $\hat{\mathbf{c}}$ are row vectors containing the parameters of a turbine and the centroid, respectively. To avoid local optimality, the clustering was replicated 500 times using new initial cluster centroid positions. The cluster quality was evaluated using the silhouette value S_i (eq. (11)) [74]

$$S_i = \frac{w_i - u_i}{\max(u_i, w_i)} \tag{11}$$

where u_i is the average distance from individual i to other individuals of the same cluster and w_i is the average distance from individual i to the individuals of the nearest neighboring cluster. According to literature [74], silhouette values greater than 0.5 indicate acceptably clustered data and values greater than 0.7 indicate well clustered data. On the other hand, for values below 0.25, absence of substantial structure in the data is suggested. The findings from this analysis were compared with computational time and accuracy of results to draw conclusions about the ideal number of clusters.

Cost models. Attempting to gather precise costs for wind power installations is a difficult endeavor due to the nature of the market, i.e. project offers rather than off-the-rack prices combined with high confidentiality. Hence, the models and data presented in this section should be understood as an estimate to distinguish between the different turbines within this study, rather than calculating commercial costs. The framework used in this study considers the total costs to consist of annuitized investment cost and operation and maintenance (O&M). For already existing turbines, only O&M were considered. The investment cost for new turbines (Table 4) was divided into turbine price and installation cost, the latter including foundations, electrical infrastructure, installation, and planning and development.

The average turbine prices in 2010 (latest value found for the Netherlands in open literature) were 1327 EUR/kW and 1970 EUR/kW for onshore (The Netherlands) and offshore (global), respectively [75]. To refer those prices to a certain turbine size, the average rated capacity in Europe in 2010 was used which is 1.8 MW onshore [76] and 3.0 MW offshore [77]. Due to increasing material requirement, turbine costs and hence prices increase with rated power. Kikuchi and Ishihara [78] found a quadratic relation between weight, i.e. material requirement, and rated power based on three turbines ranging from 2 MW to 10 MW. We use this to define a scaling factor SF (Eq. (12))

$$SF = -0.0064(P^r)^2 + 0.6983P^r - 0.3708 \tag{12}$$

where P^r is in MW. Assuming a linear relation between weight and price, the scaling factor was used to calculate the prices for turbines with different capacities according to Eq. (13)

$$p_i = \frac{SF_i}{SF_{ref}} \frac{P^r_{ref}}{P^r_i} p_{ref} \tag{13}$$

where p is the specific price in EUR/kW, i indicates the turbine type and 'ref' refers to the reference turbine. Finally, those values were updated to 2019 using historic and up-to-date data from the International Renewable Energy Agency (IRENA) [55]. The results of this analysis are summarized in Table 5.

With the price known, the installation cost can be described as a fraction f of the total cost

$$c_i^{inv} = \frac{p_i}{1 - f_i} \tag{14}$$

where c_i^{inv} is the installed cost (or total cost) for turbine i. The average installation cost of onshore turbines is around 25% of the total cost [75], i.e. average value of f is 0.25. Since the Netherlands show a rather uniform terrain, it is assumed that the installation cost is location-independent. Furthermore, it was assumed that price and installation cost scale with the turbine size equally, i.e. f is constant. As a result, f is independent of location and turbine type for onshore turbines and the average value of 0.25 was used. As opposed to onshore turbines, the installation cost of offshore turbines can depend on the location since it is a strong function of water depth and distance to coast. The European Environmental Agency investigated those effects based on a 200 MW wind farm featuring 2 MW turbines [79]. Using these data, the fraction of the installation costs on the total costs was derived as a function of water depth and distance to shore. The discrete data are provided in the

Table 5
Wind turbine prices for 2019 resulting from the model presented in Section 2.4.

	Onshore				Offshore		
	Ref	WT-1.5	WT-2.5	WT-4.5	Ref	WT-6.0	WT-9.5
Rated power [kW]	1800	1500	2500	4500	3000	6000	9500
Price [EUR/kW]	852	783	947	1041	1368	1473	1474

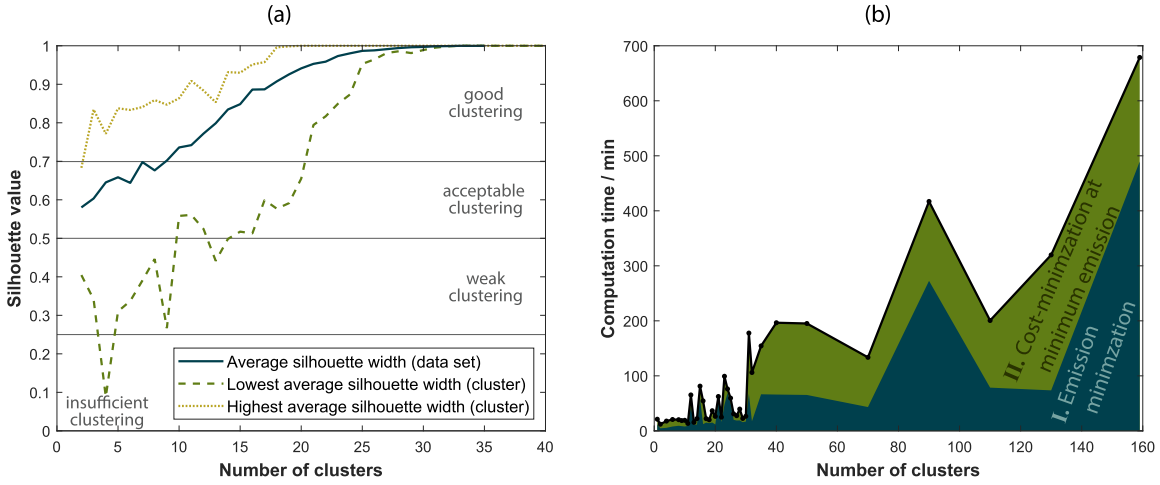

Fig. 5. Effect of the number of clusters on different parameters: (a) Average silhouette value. The data shown is the average of 20 iterations of the clustering described in Section 2.4. (b) Computation time to calculate the minimum system costs at minimum emissions. The stacked areas show the contributions of the two distinct optimization steps necessary: (1) minimization of emissions, (2) minimization of cost at minimum emissions.

supplementary material and the fitted function is given by

$$f = 10^{-5}(54860 + 128.3d - 324.8D + 0.525d^2 + 4.172Dd + 27.28D^2) \quad (15)$$

where d is the distance to coast in km and D is the water depth in m. Again, the factor f obtained via Eq. (15) is used for all offshore turbine sizes. Finally, it is important to note that the underlying data [79] are not based on a multivariate analysis but rather a combination of two univariate analyses. However, validation with the data presented by EWEA [77], i.e. average water depth of 17.4 m and average distance to shore of 27.1 km, showed that the model agrees with the numbers presented by IRENA [75].

The O&M for onshore wind power is reported to be between 11% and 30% of LCOE and tends to be higher for offshore [75]. Since adaption of best practices in operation are expected to decrease O&M in the future, 10% and 20% of the annuitized investment cost were assumed for new onshore and offshore turbines, respectively. For existing turbines, the European average of 38 EUR/kW annually [80] was used for onshore and offshore.

Evaluation of wind turbine model performance. The ideal number of wind turbine clusters can be decided by considering the computing time along with the quality of the model outcome. The latter consists of two important dimensions; firstly, the accuracy of the evaluated objective function, and secondly, the level of information about the system design which depends on the quality of the clusters. Fig. 5a shows the average silhouette value of the whole data set and the average values for the best and worst single cluster. The horizontal lines indicate the acceptability of the silhouette value as described by Kaufman and Rousseeuw [74]. While even two clusters show an acceptable average silhouette value, the worst cluster shows a rather poor value. Starting at ten clusters, also the worst cluster falls into the acceptable range and for more than 20 clusters, all clusters show a high quality. Furthermore, it is worth noting that perfect clustering ($S = 1$) is achieved at around 30 clusters, which implies that adding more clusters adds variables to the system without any gains in terms of information content.

To investigate how the computation time depends on the number of clusters, the time needed to evaluate the minimum costs at minimum emissions was computed. Here, the minimum emissions design is obtained via the ε-constraint method, i.e. optimizing for emissions and subsequently optimizing for costs while limiting the emissions to the earlier established minimum. A general trend of increasing computation time for an increasing number of clusters can be observed, albeit with significant fluctuations (see Fig. 5b). Despite those fluctuations, a strong increase can be observed from 30 to 31 clusters, which coincides with reaching a silhouette value of 1 and is suspected to be caused by the aforementioned increase of number of variables without gain of information. Combining the findings led to the choice of 20 clusters as basis for this study, given that it shows a sufficient cluster quality while maintaining a reasonable safety margin to the sharp increase in computation time with 31 clusters.

To see how curtailment affects different designs, four Pareto-optimal points, evenly spaced from emissions of 0 to 0.34 kg/kWh, were analysed for varying numbers of clusters of turbines (1, 2, 4, 6, 8, 10, 20, 30), each with continuous and discrete curtailment. Fig. 6a shows the standard deviation of the objectives (cost and emission), due to the different numbers of clusters as percentage of the average, for the Pareto-optimal designs.

Given that the standard deviation never exceeds 0.1%, it can be concluded that the number of clusters does not significantly affect the objective function; however, for a lower number of clusters the original set of turbines is not well represented (see Fig. 5a) and therefore information about the system design is limited. Furthermore, the method of curtailment seems to have little influence on the quality of the results, which was to be expected due to the high number of installed turbines. Fig. 6b shows that the computation time for unconstrained objective functions, i.e. optimization for costs or emissions without a limit on the other respective objective, is rather independent of the number of clusters and method of curtailment, while significant effects of the number of clusters can be observed for the optimization of costs with a limit on emissions. Furthermore, a striking drop in computation time

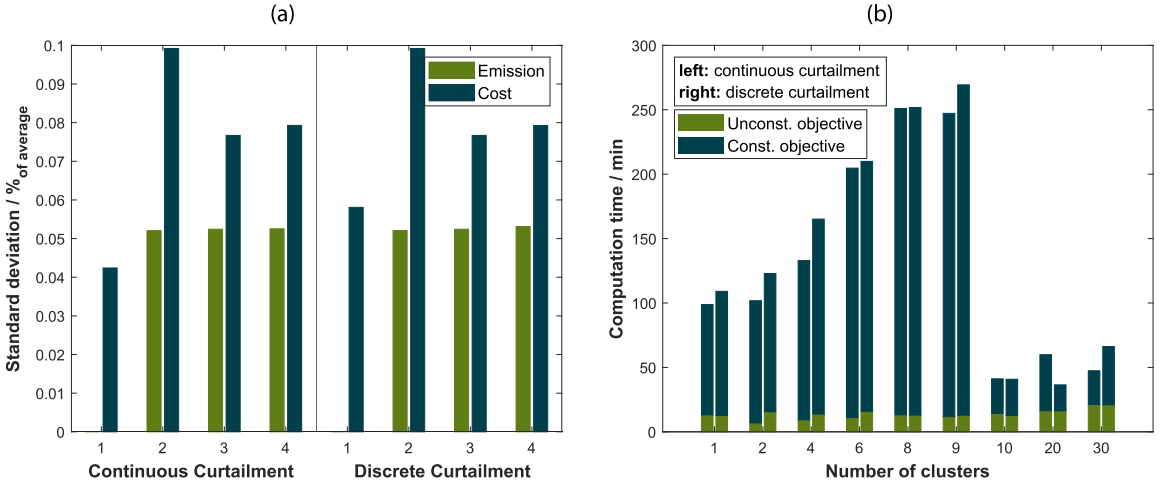

Fig. 6. Effect of the number of clusters of turbines and the method of curtailment on an multi-objective optimization using the ϵ-constraint method to produce four Pareto-optimal designs. (a) Standard deviation of the objectives (cost and emission) due to the different numbers of clusters as percentage of the average for the four Pareto-optimal designs. (b) Time required to compute the Pareto-optimal designs for different numbers of clusters.

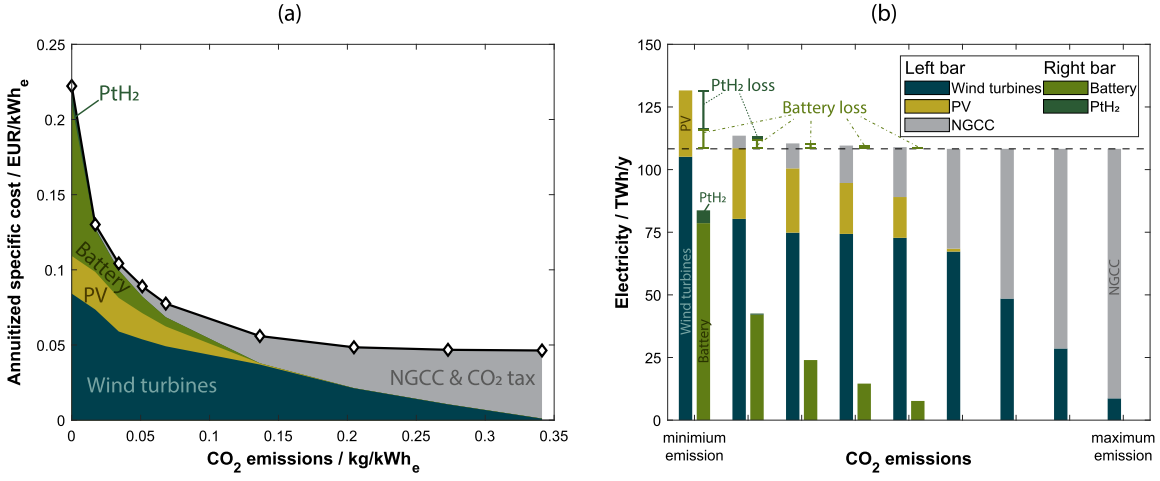

Fig. 7. (a) Cost-emission Pareto front for the base case. The colored areas show the cost contribution of different technologies. (b) Annual electricity output by technology for each Pareto-optimal design. The horizontal dashed line shows the annual electricity end-user demand.

going from nine to ten clusters can be observed. However, this behavior holds true only when using Gurobi [36], but could not be reproduced with a different commercial solver. This suggests that the computation time generally increases continuously with the number of clusters, with the exception of Gurobi finding advantageous problem structures which allow for shorter computation times despite a greater number of variables. The method of curtailment affects the computation time but no consistent trend could be identified for this test case. However, a comparison of discrete and continuous curtailment for the full-scale base case (see Section 3.1) shows significantly lower computation time with continuous curtailment. Furthermore, the finding that the method of curtailment does not significantly affect the objective function nor the system design could be confirmed (data provided in the supplementary material). Hence, continuous curtailment was used for all optimizations.

3. Results

3.1. System design for the base case

The base case considers the Dutch electricity demand but no commodity hydrogen demand. Fig. 7 shows the cost-emission Pareto front and how different technologies contribute to the total cost (Fig. 7a) and energy (Fig. 7b) for each Pareto-optimal design.

It can be observed that only the NGCC and a few wind turbines are used in the minimum cost design, which results in CO_2 emissions of 0.34 kg/kWh. Interestingly, the Pareto front is quite flat on the high-emission side, i.e. an emission reduction down to 0.14 kg CO_2/kWh (~40% reduction) is achieved with only 20% additional costs. Two factors explain this result: (1) existing wind turbines are cheap because only maintenance cost is accounted for, and (2) new wind turbines are relatively inexpensive as far as no electricity storage is needed, i.e. there is sufficient NGCC capacity to back up wind turbines at times of low wind speed. For deep decarbonization, the NGCC becomes increasingly constrained by the emission limit. This is compensated for by increasing wind turbine, solar, and battery installations. It is important to note that the installed capacity of renewables and batteries depends on the cost ratio. For cheap renewables, oversizing at the expense of increased curtailment reduces the required battery capacity while, for cheap batteries, curtailment and hence oversizing will be minimized through increased storage capacity. Finally, the PtH_2 technologies are only installed in the zero emission design and even then only at a small scale due to the high costs of electrolyzer and fuel cell and the low electricity-hydrogen-electricity round-trip efficiency (about 30%). This is amplified if stack

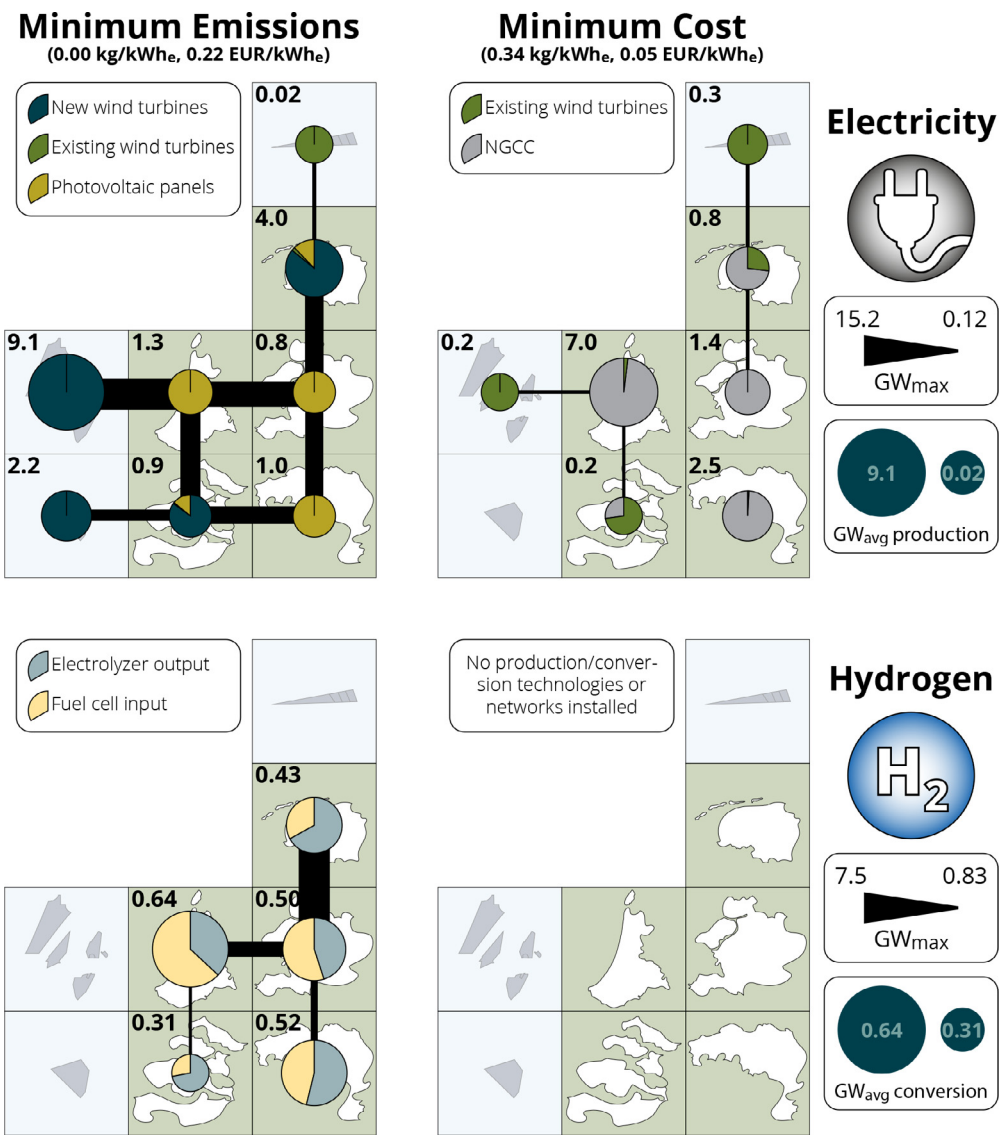

Fig. 8. Graphical summary of the base case designs for minimum emissions (left) and minimum cost (right), each separated into electricity technologies (top) and hydrogen technologies (bottom). The pie charts show the conversion technologies and the lines show the networks. The numbers in the top-left corner of each quadrant indicate the scale of the pie chart and should be read according to the legend on the right-hand side.

costs of 2000 EUR/kW are considered for electrolyzers and fuel cells, which is more representative of the situation today. In this case, PEMEC and PEMFC capacities are reduced by 81% and 64%, respectively. At the same time, the battery capacity is increased by 26% and the wind turbine peak capacity is increased by 7%. Overall, this raises the annuitized specific cost to 0.27 EUR/kWh$_e$ (+22%).

3.2. Network analysis

In order to understand the energy flows among the different regions, the electricity and hydrogen networks were fully resolved for the minimum emissions and minimum cost designs (compare with Fig. 7a). This was done in a post-processing optimization, where also the associated network costs were computed.

The initial copper-plate designs provide time-resolved information about the sources and sinks in the potential networks (see Fig. 1) but connectivity of nodes, direction of flow, and magnitude of flow are neglected. To calculate this missing information, the sources and sinks of hydrogen and electricity were re-balanced through the potential networks as to minimize the product of transported energy and transport distance as a proxy for transportation cost. The outcome of this optimization is shown in Fig. 8. Most notably, no H_2 technologies and hence no network were installed for the minimum cost design. For the technically more demanding minimum emission design, a maximum electricity grid capacity of 15.2 GW was found for the connection of the central offshore wind park. For the hydrogen network, a maximum capacity of 7.5 GW was found for the connection of the northern-most onshore node hosting the hydrogen storage. Furthermore, the network utilization of the hydrogen network is much lower compared to the electricity network. This is due to the fluctuation in hydrogen production and the lack of local storage possibilities.The renewable conversion technologies for the minimum emission design clearly show the importance of having a spatially resolved system, even if the network is modeled as a copper-plate. Three out of five onshore-nodes do not host any wind turbines as their wind profiles are inferior to other locations. Moreover, new offshore wind turbines are preferably built in the center and southern offshore-node due to lower investments costs as a result of shorter distance to shore and lower water depth.

The costs of the designed networks were calculated using values reported in literature [81] and summarized in Table 6.

Table 6
Calculation of the transportation costs for electricity and hydrogen based on the post-processed network design for the base case shown in Fig. 8. *) Taken from [81], 1 USD = 0.85 EUR.

	Electricity		Hydrogen (pipeline)	
Minimum cost*) [EUR/km-GWh]	2.3		2.1	
Maximum cost*) [EUR/km-GWh]	11.1		22.1	
	Min. CO_2	*Min. cost*	*Min. CO_2*	*Min. cost*
Transportation cost [M-EUR/y]	30.6–147.7	0.6–2.7	7.2–75.7	0
Maximum share of system cost [%]	0.61	0.05	0.31	0

Table 7
Summary of the system designs for different hydrogen demands, represented in the four columns.

Demand	Base case	50% H_2	100% H_2	150% H_2	200% H_2
Hydrogen [GWh_{LHV}/y]	0	$0.94 \cdot 10^4$	$1.89 \cdot 10^4$	$2.83 \cdot 10^4$	$3.78 \cdot 10^4$
Electricity [GWh_e/y]	$1.08 \cdot 10^5$	$1.08 \cdot 10^5$	$1.08 \cdot 10^5$	$1.08 \cdot 10^5$	$1.08 \cdot 10^5$
Total primary electricity [GWh_e/y]	$1.08 \cdot 10^5$	$1.26 \cdot 10^5$	$1.44 \cdot 10^5$	$1.61 \cdot 10^5$	$1.79 \cdot 10^5$
Cost					
Annuitized system cost [MEUR/y]	$2.41 \cdot 10^4$	$2.67 \cdot 10^4$	$3.01 \cdot 10^4$	$3.45 \cdot 10^4$	$3.93 \cdot 10^4$
Cost of hydrogen [EUR/kWh_{LHV}]	–	0.27	0.32	0.37	0.40
Installed capacity					
Wind turbines [units]	8204	8210	8216	8484	9219
Wind turbines [GW_{peak}]	31.7	34.2	39.8	47.6	53.7
Photovoltaics [GW_{peak}]	28.0	28.0	28.0	28.0	28.0
Electrolyzer [$GW_e^{in,peak}$]	8.7	14.4	18.4	22.0	27.4
Electrolyzer [$GW_{LHV}^{out,peak}$]	4.6	7.7	9.8	11.8	14.6
Fuel Cell [$GW_{LHV}^{in,peak}$]	8.6	6.1	5.2	2.7	0
Fuel Cell [$GW_e^{out,peak}$]	4.4	3.1	2.7	1.4	0
Battery [GWh_e]	431.3	501.8	576.0	637.4	726.6
Salt cavern working capacity [GWh_{LHV}]	6712.6	5572.6	5681.2	5297.0	4878.2
Salt cavern volume [m^3]	$4.30 \cdot 10^7$	$3.57 \cdot 10^7$	$3.64 \cdot 10^7$	$3.39 \cdot 10^7$	$3.12 \cdot 10^7$
System Utilization					
Primary uncurtailed electricity [GWh_e/y]	$1.82 \cdot 10^5$	$1.92 \cdot 10^5$	$2.12 \cdot 10^5$	$2.45 \cdot 10^5$	$2.70 \cdot 10^5$
Primary curtailed electricity [GWh_e/y]	$1.33 \cdot 10^5$	$1.44 \cdot 10^5$	$1.56 \cdot 10^5$	$1.74 \cdot 10^5$	$1.97 \cdot 10^5$
Renewable energy utilization [%]	73	75	73	71	73
System efficiency [%]	59	66	68	66	66
Average storage time in batteries τ^* [h]	17.5	20.2	28.3	25.6	17.2

It can be seen that for the considered system, the transportation costs account for less than 1% of the total system cost, which suggests that the copper-plate assumption is reasonable for similar studies. On the other hand, it should be noted that the maximum capacity of 15.2 GW found for the required electricity grid far exceeds the current capacity of about 3 GW. Extending the electricity grid is deemed to be a difficult endeavor (e.g. with respect to social acceptability), and therefore constitutes a potential barrier. While this aspect exceeds the scope of this work, it should be kept in mind when interpreting the results. Furthermore, it is important to notice that due to the copper-plate assumption, the spatial resolution only affects the wind turbines and photovoltaics due to the varying weather profiles, and the hydrogen storage due to its specific location in the northern-most onshore node. The location of electrolyzers, fuel cells, and batteries, however, does not affect the results.

3.3. Effect of H_2 demand on the system design and operation

In future energy systems, H_2 will be required not only for balancing electricity from renewables, but also - and mainly - for decarbonizing several other sectors [10]. To investigate the effect of a commodity hydrogen demand on the energy system design and operation, 50%, 100%, 150%, and 200% of the present hydrogen production of the Port of Rotterdam (9.44 TWh_{LHV}/y [82]) were considered. The hydrogen demand is equally distributed along the year, which is in line with considering a demand from industry and transportation. For each demand, the system was optimized for minimum cost at minimum emission considering a stand-alone case (system supplies hydrogen only, i.e. no end-user electricity demand) and an integrated case (system satisfies commodity hydrogen as well as end-user electricity demand). These two cases allow us to evaluate the benefits - if any - of sector coupling, e.g. electricity, industry, and transportation.

Table 7 and Fig. 9 show the system design for different hydrogen demands. Detailed results of the stand-alone designs are provided in Table 2 of the supplementary material.

Besides the trivial observation that increasing the hydrogen demand leads to an increase in primary electricity production, i.e. more PV and wind turbine installations, Table 7 shows that fuel cells and salt caverns decrease in size while electrolyzers and batteries increase. A better understanding of the system can be gained comparing the integrated design (Table 7) and the stand-alone design for the PtH_2 system, which is shown in Fig. 10.

For fuel cells and the salt cavern, the size decreases in the integrated design and increases in the stand-alone design until the converge eventually for high hydrogen demands. Contrary to this, the size of electrolyzers increases in both the integrated and the stand-alone designs. However, looking at the hydrogen production from the electrolyzers (see Fig. 10d), it can be seen that the production approaches the demand, implying that the amount of hydrogen converted back to electricity decreases. The behaviour of those three technologies, together with the increase in battery size, leads to the conclusion that the purpose of the PtH_2 system shifts from electricity storage to hydrogen production for high hydrogen demands. This can be explained by the higher efficiency for electricity-to-hydrogen compared to electricity-to-hydrogen-to-electricity, i.e. the primary electricity is utilized in a more efficient manner. The trade-off between PtH_2 and batteries depends on the increase in the average storage time (τ^*), and hence self-discharge losses, in the batteries. In the case at hand, τ^* varies between 17.2 h and 28.3 h. This narrow window of variation and small magnitude (i.e. hours rather than days), as well as the very pronounced shift of the PtH_2 system to hy-

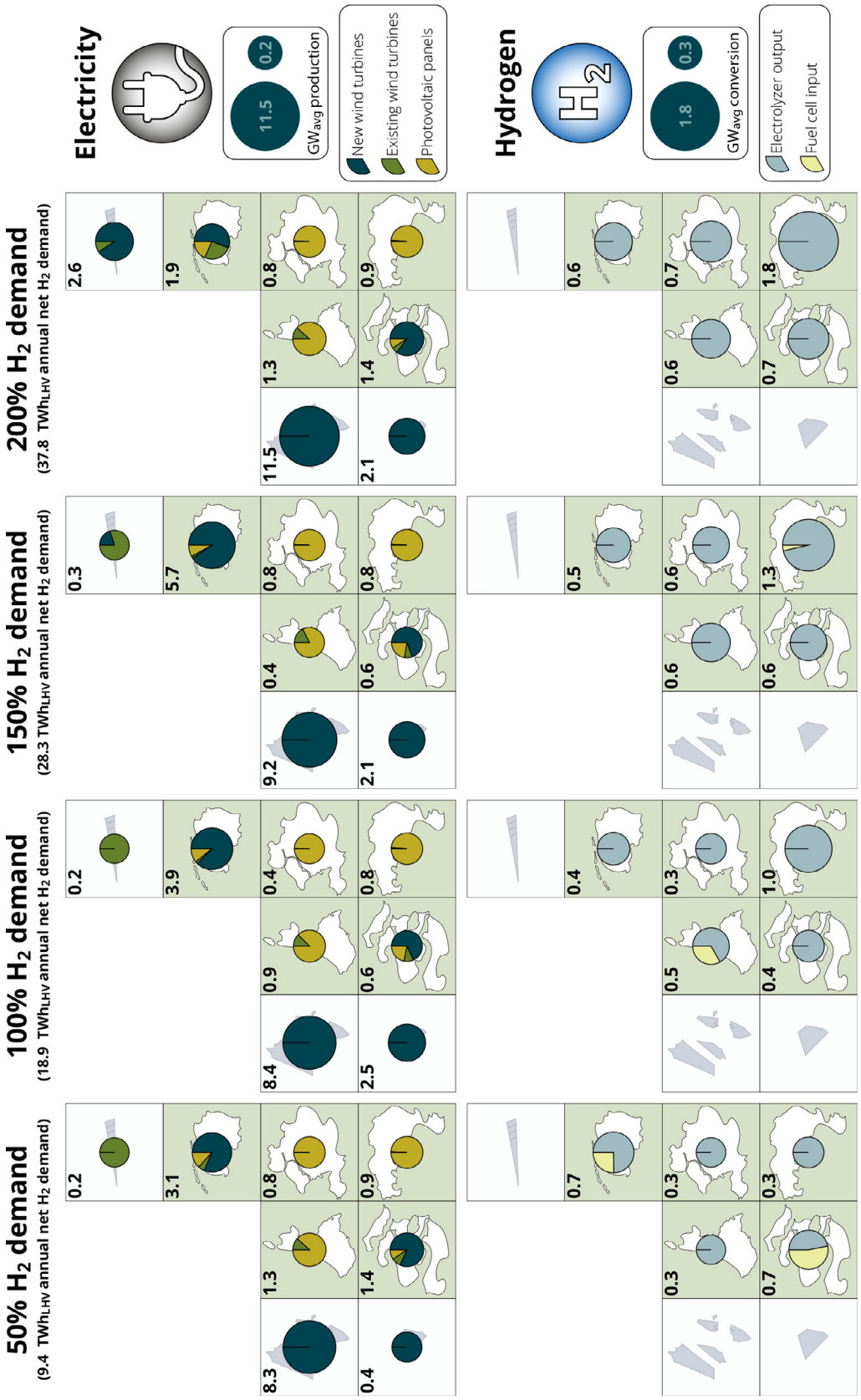

Fig. 9. Graphical summary of the integrated copper plate designs for different hydrogen demands, optimized for minimum cost at minimum emission. Each scenario is separated into electricity technologies (top) and hydrogen technologies (bottom). The pie charts show the conversion technologies. The numbers in the top-left corner of each quadrant indicate the scale of the pie chart.

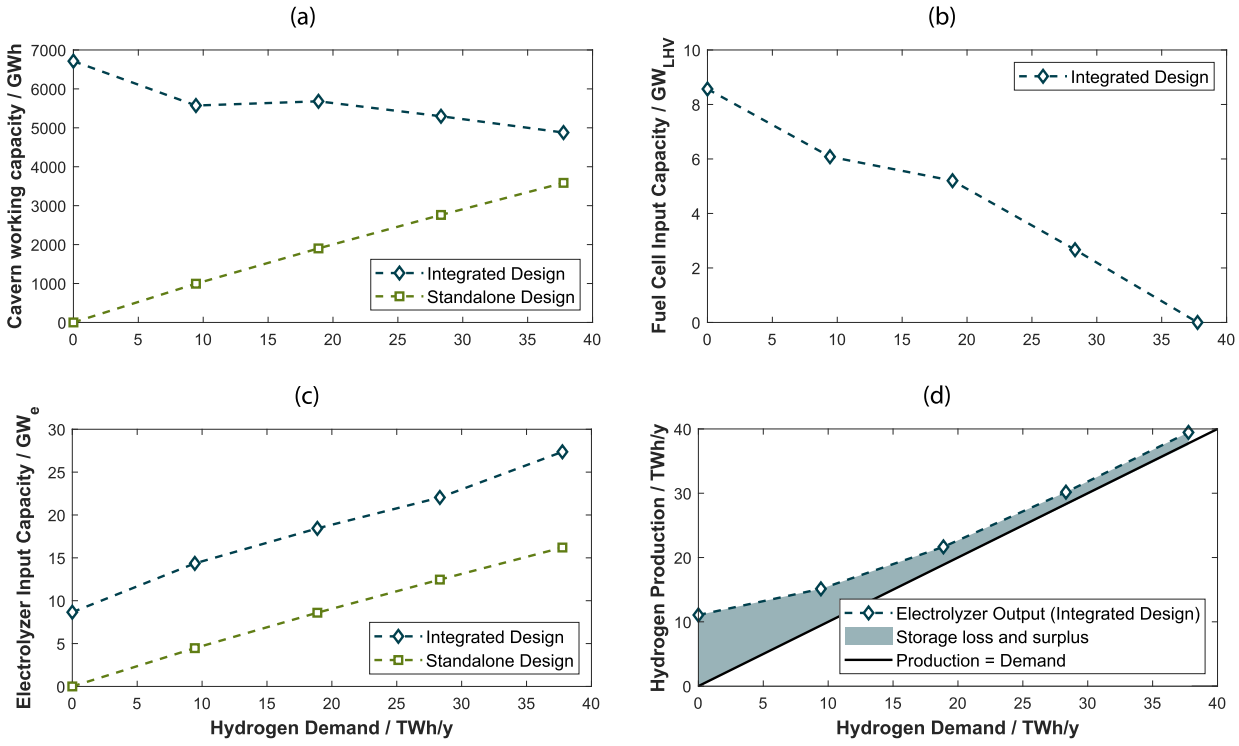

Fig. 10. Sizes of the PtH_2 technologies as a function of the hydrogen demand. (a) Cavern working capacity (b) Fuel cell input capacity (c) Electrolyzer input capacity (d) Hydrogen production.

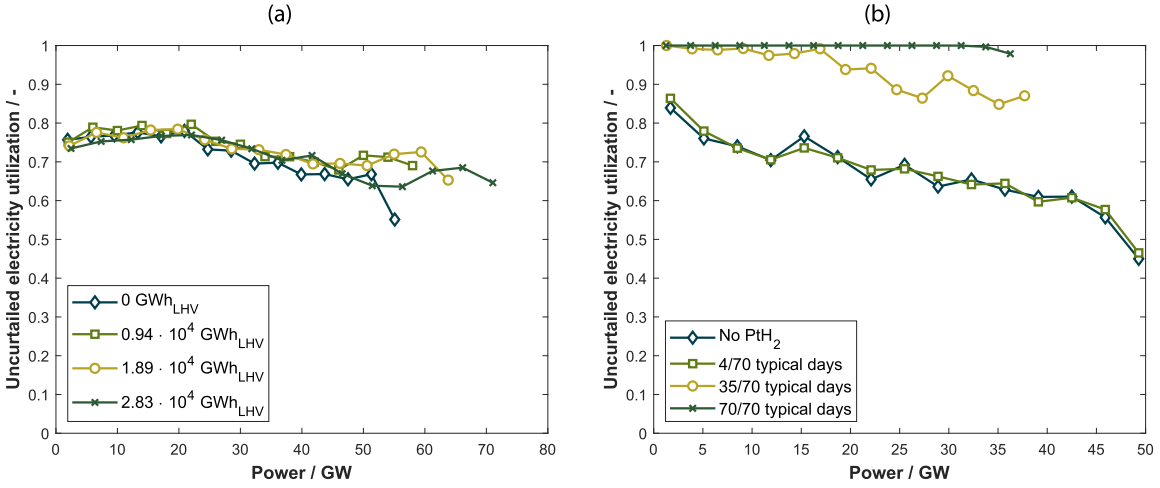

Fig. 11. Utilization of renewables as a function of the power spectrum. (a) Integrated designs for a full year, 20 typical days, and different hydrogen demands. (b) Base case for 70 days and different number of typical days.

drogen production indicate that the system does not experience strong seasonality, which is in line with typical electricity profiles and constant commodity hydrogen demand.

The utilization of primary electricity does not significantly depend on the hydrogen demand (see Fig. 11a).

An increase in utilization can only be observed for peak-power production, which indicates that hydrogen is mainly produced at those times. Further evidence for this conclusion lies in the installed capacity of the electrolyzer. Fig. 10c and d show that the electrolyzer capacity installed in the integrated design is significantly larger than in the stand-alone design, despite similar production for high hydrogen demands. The reason for this is that the electrolyzer in the integrated design mainly utilizes power peaks and hence needs a greater capacity, while the electrolyzer in the stand-alone design utilizes the full spectrum and extreme events can be curtailed in favor of a smaller installed capacity. To facilitate the former behavior, and therefore operate properly in a power-integrated system, electrolyzers require significant operation flexibility.

It should be noted that this operation flexibility of the PtH_2 technologies is affected by the chosen modeling approach of typical days. Through using a limited set of fixed operating patterns to model the full year, the flexibility is significantly constrained. While the electrolyzer and the fuel cell can react to peaks in supply or demand, i.e. from a technical point of view they possess sufficient flexibility, the modeling strategy allows only for 20 ways of doing so (20 operating patterns according to 20 typical days).

To better understand the impact of this, the base case system (without hydrogen demand) was analyzed for a reduced time horizon of 70 days, which allowed to simulate the PtH_2 technologies with high degrees of flexibility by increasing the number of typical days used to model

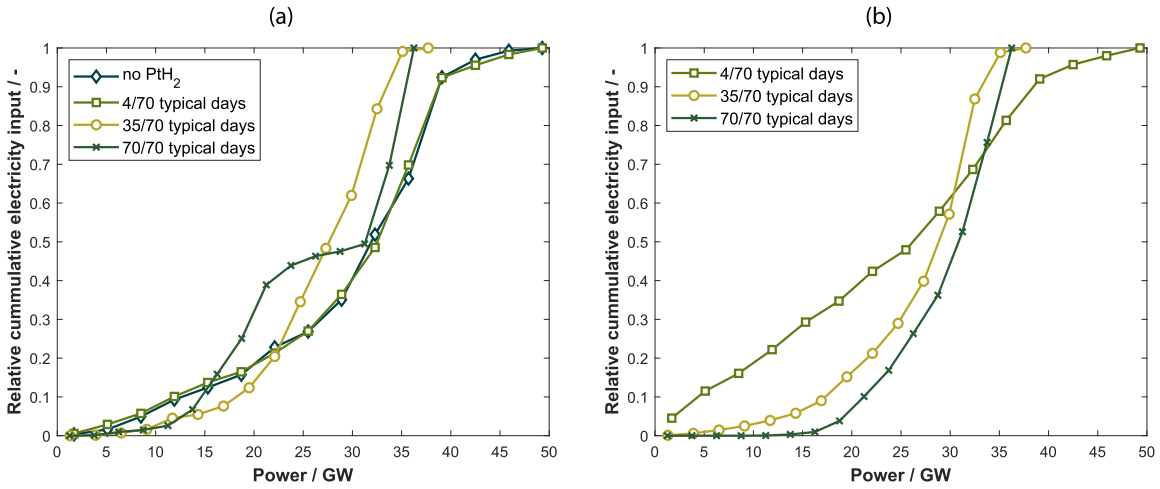

Fig. 12. Power spectrum utilization of (a) batteries and (b) electrolyzers for varying electrolyzer flexibility based on optimizations with a time horizon of 70 days and different number of typical days.

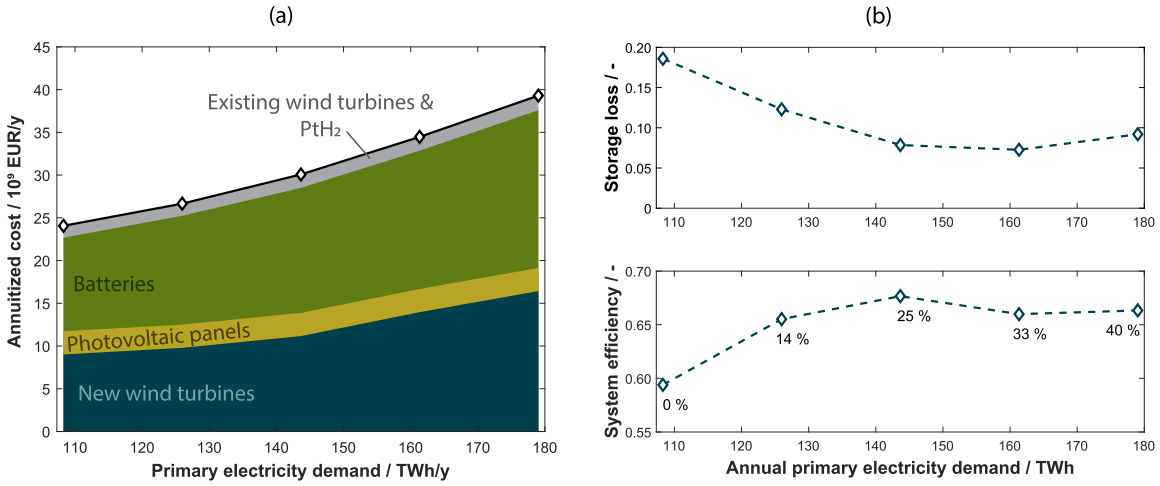

Fig. 13. Different parameters as a function of the annual primary electricity demand. (a) System cost including a cost breakdown. (b) Utilization, storage loss, and system efficiency. The annotations in the bottom graph show the share of primary electricity demand caused by the hydrogen demand.

them. The more typical days are used, the more the PtH_2 technologies are free to operate according to the demand/input profiles; no numerical constraints are present if the number of typical days equals the time horizon, i.e. 70 days. All other technologies are modeled with full time resolution and are therefore not affected. An analysis with four typical days was run to represent the situation for the full year, as the ratio between typical days and time horizon is the same. However, potential effects on seasonality cannot be observed on this short time horizon.

Fig. 11 b shows how the utilization, especially for the high end of the power spectrum, increases with increasing number of typical days. A result of the increased utilization is that the installed capacity of wind turbines and PV decreases, making the power spectrum narrower. However, while almost perfect utilization over the full spectrum is achieved for 70 typical days, adding PtH_2 technologies with only 4 typical days has hardly any effect. This suggests that the impact of hydrogen demand on the utilization (Fig. 11a) could be higher without the constraint of typical days, calling for more elaborate modeling approaches.

The operation of the PtH_2 technologies is not only affected by the modeling approach but also by the interaction with other technologies. Looking at which parts of the power spectrum are used to charge the batteries or drive the electrolyzers (Fig. 12), it can be seen that the two technologies are complementary if the electrolyzer is free to operate according to the full time profiles (yet within the technological constraints considered).

While hydrogen is produced at times of high-power peaks, batteries tend to use the middle part of the power spectrum for charging. If the flexibility of the electrolyzer gets constrained, the regimes mix up, i.e. the electrolyzer increasingly utilizes the lower parts of the power spectrum while battery charging shifts towards the higher end of the spectrum (note that batteries are always modeled with full time resolution). This is also reflected in the battery size and system costs; the effect of adding PtH_2 with four typical days to the system is negligible, reducing the battery size from 616 GWh to 614 GWh and the system cost from 1.299 EUR/kWh to 1.297 EUR/kWh. However, increasing the typical days from four to 70 reduces the battery size to 16.25 GWh and the system cost to 0.54 EUR/kWh.

It can be noted that the cost of hydrogen in the full-scale design found in Table 7, which is calculated as the added cost (compared to the base case) per unit added hydrogen demand, increases with increasing hydrogen demand. The origin of this trend lies in the system operation and is explained in the following.

At first, the role of hydrogen transitions from electricity storage to supply of demand (Fig. 10d). As a result, the storage losses drop (Fig. 13b) due to decreasing fuel cell conversion losses (Fig. 14). Due

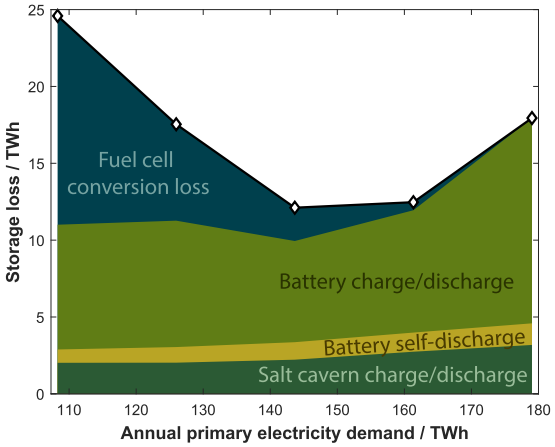

Fig. 14. Absolute annual storage loss for the different hydrogen demand scenarios.

to the rather constant utilization, this drop leads to an increase in system efficiency. The long-term storage task of PtH_2 is taken over by the batteries, increasing the average time of electricity stored. Once hydrogen is not used for electricity storage anymore, no more gains can be obtained through minimizing the losses from the fuel cell by reducing its operation and hence the system needs to expand more radically. This is mainly achieved through installations of new wind turbines and batteries (Fig. 13a). The batteries, while increasing their average time of electricity stored at first, decrease this time now as a result of more energy being stored for shorter periods of time. This leads to an increase in charge and discharge losses while the self-discharge stays rather constant (Fig. 14). However, the increase is proportionate to the increase in primary energy demand and hence, the relative storage loss remains rather constant around 10%. Consequently, the system efficiency stabilizes, which shows that the increase in primary electricity demand is entirely covered by system expansion. However, maintaining the efficiency becomes increasingly costly due to the increasing battery requirements, explaining the increase of cost of hydrogen. This let us conclude that the more hydrogen needs to be produced (continuously) from non-dispatchable renewables, the higher the total and specific cost.

4. Conclusion and recommendations

In this work, we present a spatially and temporally resolved MILP optimization of a fully renewable, wind-dominated, zero-emission energy system to supply the Dutch electricity and hydrogen demand. The optimization's purpose is to understand the respective roles of, but also the interaction between, PtH_2, batteries, and conversion technologies in the system. This is possible thanks to the detailed underlying technology models and the hourly resolution over an analysis period of one year. While most of the technology models used in the optimization framework have been published elsewhere, an approach to model large wind turbine portfolios was developed and presented in this work. We show that the applied clustering algorithm allows to reduce the portfolio size without significant loss of information. Furthermore, a cost model for offshore wind turbines, accounting for distance to shore and water depth is included in the wind turbine model.

To pinpoint the role of hydrogen and its related technologies, different hydrogen demands were applied. The following conclusions can be drawn - it should be noted that the findings are specific to cases with similar boundary conditions (wind-dominated systems and similar cost assumptions) and should not be generalized or blindly applied to other cases:

- With increasing hydrogen demand, the PtH_2 system is preferably used to produce hydrogen, rather than storing electricity, i.e. hydrogen is not converted back to electricity. Moreover, the cost of hydrogen increases with increasing hydrogen demand as a result of increasingly costly system expansion.
- Electrolyzers preferably utilize high-power peaks. Complementary, batteries tend to cover moments of minor over-production.
- Due to the preferred utilization of high-power peaks, PtH_2 technologies are best operated when free to follow the real hourly profile while considering the full year horizon. From a modeling point of view, this calls for new methods for time discretization within MILP optimization, where an hourly resolved full year horizon can be handled without recurring to super computing facilities. From a technical point of view, it calls for electrolyzers to flexibly adapt their operation to the time-dependent specifics of the system.
- A steady-state operation of electrolyzers, enabled by batteries balancing the electricity production, was not found to be optimal on a national level. However, individual interests of different actors were not taken into account in this work, i.e. steady-state operation could be beneficial for certain parties at the expense of diverging from the national optimum.
- We recommend to critically reassess the role of H_2 as storage medium for electricity in a hydrogen economy. While this work is not suited as basis for final decisions as it lacks details about regulatory and economic effects as well as a large enough set of different H_2 supply chains, it clearly shows that the conversion of H_2 to electricity to balance the grid is not favored if a commodity hydrogen demand is present.

Declaration of Competing Interest

The authors declare that they have no known competing financial interests or personal relationships that could have appeared to influence the work reported in this paper.

CRediT authorship contribution statement

Lukas Weimann: Conceptualization, Methodology, Formal analysis, Visualization, Writing - original draft. **Paolo Gabrielli:** Software, Writing - review & editing. **Annika Boldrini:** Formal analysis. **Gert Jan Kramer:** Conceptualization, Visualization, Writing - review & editing. **Matteo Gazzani:** Conceptualization, Visualization, Supervision, Funding acquisition, Writing - review & editing.

Acknowledgments

ACT ELEGANCY, Project no. 271498, has received funding from DETEC (CH), FZJ/PtJ (DE), RVO (NL), Gassnova (NO), BEIS (UK), Gassco AS and Statoil Petroleum AS, and is cofunded by the European Commission under the Horizon 2020 programme, ACT Grant Agreement no. 691712.

Appendix A. Model formulation

This section reports the detailed problem formulation, as an addition to Section 2.2. The problem features three main dimensions: (i) time $t \in \mathcal{T}$, where $\mathcal{T} = [1, T]$ is the set of all time instances and $T = 8760$ is the analysis horizon, (ii) space as discrete nodes $n \in \mathcal{N}$, where $\mathcal{N}$ is the set of all nodes and $N = 8$ is the number of nodes, and (iii) technologies $i \in \mathcal{M}$, where $\mathcal{M}$ is the set of all technologies.

A1. Objective functions

The objective functions of the optimization problem are the total annual cost of the system, χ_c, or the total annual CO_2 emissions, χ_e. The former is compiled as the sum of the annual capital cost, J_c, the annual operation cost, J_o, and the annual maintenance cost, J_m.

$$\chi_c = J_c + J_o + J_m \tag{16}$$

The annual capital cost is expressed as

$$J_{\mathrm{c}} = \sum_{j\in\mathcal{N}} \sum_{i\in\mathcal{M}} \left(\lambda_i S_{i,j} + \mu_i\right) a_i \tag{17}$$

where λ_i and μ_i represent the variable and fixed cost coefficients for the i-th technology. The equivalent annual investment cost is computed through the annuity factor a, where an interest rate of 10% is considered. The annual operation cost is calculated based on the amount of imported electricity during the year:

$$J_{\mathrm{o}} = \sum_{n\in\mathcal{N}} \sum_{t\in\mathcal{T}} p_e U_{n,t} \tag{18}$$

where p_e is the price of electricity, i.e. the LCOE of an NGCC (40 EUR/MWh). The annual maintenance cost is given as a fraction ψ of the annual capital cost

$$J_{\mathrm{m}} = \sum_{n\in\mathcal{N}} \sum_{i\in\mathcal{M}} \psi_i J_{c,n,i} \tag{19}$$

Since no carbon-emitting technologies are considered in the system, χ_e is entirely determined by the amount of electricity imported

$$\chi_e = \sum_{n\in\mathcal{N}} \sum_{t\in\mathcal{T}} e U_{n,t} \tag{20}$$

where e is the emission factor of imported electricty, i.e. the emission factor of an NGCC (371 g/kWh).

A2. Decision variables

The following decision variables are obtained as outputs of the optimization problem:

i. The size of the installed technologies, $S \in \mathbb{R}^N$ (except for wind turbines, where $S \in \mathbb{N}^N$ since the size is expressed as number of turbines). Note that determining S (greater than zero if a technology is selected) also implies selecting the technologies.
ii. The on/off status for PEMEC and PEMFC, $\mathbf{x} \in \{0,1\}^{N\times T}$.
iii. The input power, $\mathbf{F} \in \mathbb{R}^{N\times T}$, and output power, $\mathbf{P} \in \mathbb{R}^{N\times T}$, of the available technologies.
iv. The stored energy in the storage technologies, $\mathbf{E} \in \mathbb{R}^{N\times T}$
v. The output power of the NGCC, modeled as imported electrical power $\mathbf{U} \in \mathbb{R}^{N\times T}$.

The operation of PEMEC, PEMFC, and the H_2 storage (decision variables ii and part of iii) is modeled through 20 typical design days unless stated otherwise, whereas the operation of all other conversion and storage technologies and the imported electricity (decision variable iv and v) are determined at every hour of the year.

A3. Constraints

The optimization constraints can be divided into two categories:

i. *Performance of conversion and storage technologies.* Three different types of technologies are considered in the framework, namely generic conversion technologies, renewable conversion technologies (solar and wind), and storage technologies. The performance of each type is formulated in a different way. However, they all have a constrained size

$$S_i^{\min}\sigma_{i,n} \le S_{i,n} \le S_i^{\max}\sigma_{i,n} \tag{21}$$

where $S_{i,n}$ is the size of technology i at node n, $\sigma_{i,n}$ is a binary determining whether technology i is installed at node n, and $S_i^{\min}$ and $S_i^{\max}$ are the user-defined minimum and maximum sizes of technology i. Note that the minimum and maximum sizes could easily be defined per node within the proposed optimization framework if necessary.

The performance of generic conversion technologies is described by linear or piecewise linear functions

$$P_{t,i,n,k} \le f_{i,k}(F_{t,i,n}, S_{i,n}, x_{t,i,n}, \Theta_{i,k}) \tag{22}$$

where P is the output, f is the linear function, F is the fuel input (e.g. in the form of hydrogen), x is the ON/OFF status, and Θ is the set of performance parameters; t, i, n, and k indicate the time, technology, node, and energy carrier produced, respectively. The fuel input is constrained by minimum and maximum values which are a function of the size.

$$F_i^{\min}(S_{i,n}) \le F_{t,i,n} \le F_i^{\max}(S_{i,n}) \tag{23}$$

Details about the linear functions f, $F_i^{\min}$, and $F_i^{\max}$ for different technologies can be found in the references provided in the respective paragraph in Section 2.3.

For solar and wind power installations, the power output depends on the solar/wind availability and the technology efficiency. Note that as the solar/wind input is not optimized but assigned by the meteorologic conditions, there is no need to adopt linear input-output equations. Moreover, curtailing the power output is permitted by the performance constraint

$$P_{t,i,n} \le P_{t,i,n}^{\max}(S_{i,n}, \Theta_i, \Phi_{t,n}) \tag{24}$$

where $P^{\max}$ is the maximum power output for given weather conditions Φ at node n and installed size S.

The energy content $E_{t,i,n}$ of storage technology i at node n and time t can be described as

$$E_{t,i,n} = E_{t-1,i,n}(1-\Delta) - \Pi S_{i,n} g_{t,i,n}(T^{\mathrm{amb}}) + \eta^{\mathrm{in}} E_{t,i,n}^{\mathrm{in}} - \frac{1}{\eta^{\mathrm{out}}} E_{t,i,n}^{\mathrm{out}} \tag{25}$$

where Δ and Π are self-discharge coefficients, g accounts for the influence of the ambient temperature T^{amb} (if relevant), and η^{in} and η^{out} are the charging and discharging efficiency, respectively. Furthermore, size and periodicity constraints have to be fulfilled

$$0 \le E_{t,i,n} \le S_{i,n} \tag{26}$$

$$E_0 = E_T \tag{27}$$

where T is the last time instance of the analyzed period. Finally, the maximum charging rate P^{in} and discharging rate P^{out} is limited as

$$P_{t,i,n}^{\mathrm{in}} \le \frac{S_{i,n}}{\tau_i^{\mathrm{in}}} \tag{28}$$

$$P_{t,i,n}^{\mathrm{out}} \le \frac{S_{i,n}}{\tau_i^{\mathrm{out}}} \tag{29}$$

where $\tau^{\mathrm{in/out}}$ is the number of time intervals required to completely charge (in) or discharge (out) the storage medium.

ii. *Energy balances.* The considered energy carriers are electricity and hydrogen. In particular, electricity can be produced by wind turbines, PV, and fuel cells, imported (from a hypothetical NGCC-plant), stored in batteries, and consumed by electrolyzers. Hydrogen can be produced by electrolyzers, stored in salt caverns, and consumed by fuel cells. Both energy carriers can be delivered to supply an end-user demand. The sum of imported and generated power must equal the used power for all energy carriers k, for all time intervals $t \in \{1, T\}$:

$$\sum_{n\in\mathcal{N}} \left[\sum_{i\in\mathcal{M}} \left(P_{k,n,i,t} - F_{k,n,i,t}\right) + U_{k,n,t} - L_{k,n,t} \right] = 0 \tag{30}$$

Here, i indicates the i-th technology, n indicates the n-th node, U the imported energy, P the generated energy, F the energy consumed by storage or conversion technologies, and L the end-users demand.

A4. Network design

For the post-processing network design, a second linear program (LP) was compiled to minimize the objective χ_{NW}

$$\chi_{\mathrm{NW}} = \sum_{\substack{m\in\mathcal{N}\\ m\neq n}} \sum_{\substack{n\in\mathcal{N}\\ n\neq m}} \left(D_{k,n,m} \sum_{t\in\mathcal{T}} \xi_{k,n,m,t} \right) \tag{31}$$

where the decision variable $\xi_{k,n,m,t}$ is the flow of energy carrier k from node n to node m at time t, and $D_{k,n,m}$ is the distance between the nodes for a certain energy carrier. This LP is subject to the following constraints

$$\xi_{k,n,m,t} - \xi_{k,m,n,t} + \sum_{i \in \mathcal{M}} \left(P_{k,n,i,t} - F_{k,n,i,t} \right) + U_{k,n,t} - L_{k,n,t} = 0 \tag{32}$$

$$\xi_{n,m,t} \geq 0 \quad \forall \quad (n,m) \in \mathcal{N}, t \in \mathcal{T} \tag{33}$$

$$\xi_{k,n,m,t} = 0 \quad \forall \quad \alpha_{n,m} = 0 \tag{34}$$

where $\alpha_{n,m}$ is the connectivity between nodes n and m. Note that P, F, U and L are given by the energy system optimization and the only decision variable is ξ.

Appendix B. Concepts and terminology

Average time of electricity stored in batteries. In order to have a measure that allows to compare the operation of batteries in different scenarios, the concept of average time of electricity stored, τ^*, is introduced. It describes the time that a unit of electricity is stored on average in order to justify the total self-discharge compared to the total input. The self-discharge loss L_t^{SDC} after t periods for an initial energy input E_0^{in} at $t = 0$ can be formulated as

$$L_t^{\text{SDC}} = \eta^{\text{in}} E_0^{\text{in}} \left(1 - (1-\Delta)^t\right) = \eta^{\text{in}} E_0^{\text{in}} \left(1 - \lambda^t\right) \tag{35}$$

where Δ and η^{in} are the self-discharge coefficient and the charging efficiency, respectively. This expression can be abstracted to an annual balance

$$\sum_t L_t^{\text{SDC}} = L_{\text{tot}}^{\text{SDC}} = \eta^{\text{in}} E_{\text{tot}}^{\text{in}} \left(1 - \lambda^{\tau^*}\right) \tag{36}$$

where $E_{\text{tot}}^{\text{in}}$ is the sum of all electricity input in the analyzed time period. From this formulation, τ^* can be extracted as

$$\tau^* = \frac{\log\left(1 - \frac{L_{\text{tot}}^{\text{SDC}}}{\eta^{\text{in}} E_{\text{tot}}^{\text{in}}}\right)}{\log(\lambda)} \tag{37}$$

This must not be mistaken with the storage periodicity, e.g. $\tau^* = 24$ does not necessarily imply a profile with daily periodicity.

Curtailment. The act of reducing the power delivery from PV and wind turbines, i.e. the curtailed output is less than the maximum output allowed by the weather conditions. As a parameter, it describes the share of electricity *not* exploited.

Renewable energy utilization. The share of electricity from PV and wind turbines that is actually delivered. The sum of curtailment and utilization is 1.

Uncurtailed power. The maximum power output from PV and wind turbines for given weather conditions.

Primary electricity demand. The sum of electricity demand and electricity-equivalent hydrogen demand. The electricity-equivalent hydrogen demand is calculated using the electrolyzer efficiency reported in Table 2.

System efficiency. The fraction of primary electricity demand over uncurtailed power.

Conversion of monetary units. 1 USD = 0.85 EUR.

Supplementary material

Supplementary material associated with this article can be found, in the online version, at 10.1016/j.adapen.2021.100032

References

[1] IPCC. Global Warming of 1.5 °C. An IPCC Special Report on the impacts of global warming of 1.5 °C above pre-industrial levels and related global greenhouse gas emission pathways, in the context of strengthening the global response to the threat of climate change, sustainable development, and efforts to eradicate poverty. Tech. Rep.; 2018.

[2] Staffell I, Scamman D, Velazquez Abad A, Balcombe P, Dodds PE, Ekins P, Shah N, Ward KR. The role of hydrogen and fuel cells in the global energy system. Energy Environ Sci 2019;12:463–91. doi:10.1039/c8ee01157e.

[3] Strachan N, Balta-Ozkan N, Joffe D, McGeevor K, Hughes N. Soft-linking energy systems and GIS models to investigate spatial hydrogen infrastructure development in a low-carbon UK energy system. Int J Hydrog Energy 2009;34:642–57. doi:10.1016/j.ijhydene.2008.10.083.

[4] Endo E. Market penetration analysis of fuel cell vehicles in Japan by using the energy system model MARKAL. Int J Hydrog Energy 2007;32:1347–54. doi:10.1016/j.ijhydene.2006.10.015.

[5] Dodds PE, Ekins P. A portfolio of powertrains for the UK: an energy systems analysis. Int J Hydrog Energy 2014;39:13941–53. doi:10.1016/j.ijhydene.2014.06.128.

[6] Ball M, Wietschel M, Rentz O. Integration of a hydrogen economy into the German energy system: an optimising modelling approach. Int J Hydrog Energy 2007;32:1355–68. doi:10.1016/j.ijhydene.2006.10.016.

[7] Contreras A, Guervós E, Posso F. Market penetration analysis of the use of hydrogen in the road transport sector of the Madrid region, using MARKAL. Int J Hydrog Energy 2009;34:13–20. doi:10.1016/j.ijhydene.2008.10.031.

[8] Capros P, Tasios N, De Vita A, Mantzos L, Paroussos L. Model-based analysis of decarbonising the EU economy in the time horizon to 2050. Energy Strategy Rev 2012;1:76–84. doi:10.1016/j.esr.2012.06.003.

[9] Capros P, Tasios N, De Vita A, Mantzos L, Paroussos L. Transformations of the energy system in the context of the decarbonisation of the EU economy in the time horizon to 2050. Energy Strategy Rev 2012;1:85–96. doi:10.1016/j.esr.2012.06.001.

[10] Sgobbi A, Nijs W, De Miglio R, Chiodi A, Gargiulo M, Thiel C. How far away is hydrogen? Its role in the medium and long-term decarbonisation of the European energy system. Int J Hydrog Energy 2016;41:19–35. doi:10.1016/j.ijhydene.2015.09.004.

[11] Samsatli S, Samsatli NJ. A multi-objective MILP model for the design and operation of future integrated multi-vector energy networks capturing detailed spatio-temporal dependencies. Appl Energy 2018;220:893–920. doi:10.1016/j.apenergy.2017.09.055.

[12] Zhang Q, Martín M, Grossmann IE. Integrated design and operation of renewables-based fuels and power production networks. Comput Chem Eng 2019;122:80–92. doi:10.1016/j.compchemeng.2018.06.018.

[13] Marchenko OV, Solomin SV. Modeling of hydrogen and electrical energy storages in wind/PV energy system on the Lake Baikal coast. Int J Hydrog Energy 2017;42:9361–70. doi:10.1016/j.ijhydene.2017.02.076.

[14] Zhang W, Maleki A, Rosen MA, Liu J. Optimization with a simulated annealing algorithm of a hybrid system for renewable energy including battery and hydrogen storage. Energy 2018;163:191–207. doi:10.1016/j.energy.2018.08.112.

[15] Zhang W, Maleki A, Rosen MA, Liu J. Sizing a stand-alone solar-wind-hydrogen energy system using weather forecasting and a hybrid search optimization algorithm. Energy Convers Manag 2019;180:609–21. doi:10.1016/j.enconman.2018.08.102.

[16] Kalinci Y, Hepbasli A, Dincer I. Techno-economic analysis of a stand-alone hybrid renewable energy system with hydrogen production and storage options. Int J Hydrog Energy 2015;40:7652–64. doi:10.1016/j.ijhydene.2014.10.147.

[17] Schnuelle C, Wassermann T, Fuhrlaender D, Zondervan E. Dynamic hydrogen production from PV & wind direct electricity supply—Modeling and techno-economic assessment. Int J Hydrog Energy 2020;45:29938–52. doi:10.1016/j.ijhydene.2020.08.044.

[18] Bødal EF, Mallapragada D, Botterud A, Korpås M. Decarbonization synergies from joint planning of electricity and hydrogen production: a Texas case study. Int J Hydrog Energy 2020;45:32899–915. doi:10.1016/j.ijhydene.2020.09.127.

[19] Welder L, Ryberg DS, Kotzur L, Grube T, Robinius M, Stolten D. Spatio-temporal optimization of a future energy system for power-to-hydrogen applications in Germany. Energy 2018;158:1130–49. doi:10.1016/j.energy.2018.05.059.

[20] Ishaq H, Dincer I, Naterer GF. Performance investigation of an integrated wind energy system for co-generation of power and hydrogen. Int J Hydrog Energy 2018;43:9153–64. doi:10.1016/j.ijhydene.2018.03.139.

[21] Khalid F, Dincer I, Rosen MA. Analysis and assessment of an integrated hydrogen energy system. Int J Hydrog Energy 2016;41:7960–7. doi:10.1016/j.ijhydene.2015.12.221.

[22] Koleva M, Guerra OJ, Eichman J, Hodge B-M, Kurtz J. Optimal design of solar-driven electrolytic hydrogen production systems within electricity markets. J Power Sources 2021;483:229183. doi:10.1016/j.jpowsour.2020.229183. https://www.sciencedirect.com/science/article/pii/S0378775320314749

[23] Xiao P, Hu W, Xu X, Liu W, Huang Q, Chen Z. Optimal operation of a wind-electrolytic hydrogen storage system in the electricity/hydrogen markets. Int J Hydrog Energy 2020;45(46):24412–23. doi:10.1016/j.ijhydene.2020.06.302. https://www.sciencedirect.com/science/article/pii/S036031992032512X

[24] Apostolou D. Optimisation of a hydrogen production - storage - re-powering system participating in electricity and transportation markets. Acase study for Denmark. Appl Energy 2020;265:114800. doi:10.1016/j.apenergy.2020.114800. https://www.sciencedirect.com/science/article/pii/S0306261920303123

[25] Guinot B, Montignac F, Champel B, Vannucci D. Profitability of an electrolysis based hydrogen production plant providing grid balancing services. Int J Hydrog Energy 2015;40(29):8778–87. doi:10.1016/j.ijhydene.2015.05.033. https://www.sciencedirect.com/science/article/pii/S0360319915011775

[26] Parra D, Gillott M, Walker GS. The role of hydrogen in achieving the decarbonization targets for the UK domestic sector. Int J Hydrog Energy 2014;39:4158–69. doi:10.1016/j.ijhydene.2014.01.023.

[27] Pérez-Uresti SI, Martín M, Jiménez-Gutiérrez A. Superstructure approach for the design of renewable-based utility plants. Comput Chem Eng 2019;123:371–88. doi:10.1016/j.compchemeng.2019.01.019.

[28] Sunny N, Mac Dowell N, Shah N. What is needed to deliver carbon-neutral heat using hydrogen and CCS? Energy Environ Sci 2020;13:4204–24. doi:10.1039/D0EE02016H.

[29] Gabrielli P, Charbonnier F, Guidolin A, Mazzotti M. Enabling low-carbon hydrogen supply chains through use of biomass and carbon capture and storage: a Swiss case study. Appl Energy 2020;275:115245. doi:10.1016/j.apenergy.2020.115245.

[30] Hansen K, Breyer C, Lund H. Status and perspectives on 100% renewable energy systems. Energy 2019;175:471–80. doi:10.1016/j.energy.2019.03.092.

[31] Gabrielli P, Poluzzi A, Kramer GJ, Spiers C, Mazzotti M, Gazzani M. Seasonal energy storage for zero-emissions multi-energy systems via underground hydrogen storage. Renew Sustain Energy Rev 2020;121. doi:10.1016/j.rser.2019.109629.

[32] Gabrielli P, Gazzani M, Mazzotti M. Electrochemical conversion technologies for optimal design of decentralized multi-energy systems: modeling framework and technology assessment. Appl Energy 2018;221:557–75. doi:10.1016/j.apenergy.2018.03.149.

[33] Juez-Larré J, van Gessel S, Dalman R, Remmelts G, Groenenberg R. Assessment of underground energy storage potential to support the energy transition in the Netherlands. First Break 2019;37:57–66.

[34] MATLAB. Version 9.4 (R2018a). Natick, Massachusetts: The MathWorks Inc; 2018.

[35] Löfberg J. Yalmip : a toolbox for modeling and optimization in matlab. In: Proceedings of the CACSD conference, Taipei, Taiwan; 2004.

[36] Gurobi. Version 9.0.0. Gurobi Optimization, LLC; 2000.

[37] Gabrielli P, Gazzani M, Martelli E, Mazzotti M. Optimal design of multi-energy systems with seasonal storage. Appl Energy 2018;219:408–24. doi:10.1016/j.apenergy.2017.07.142.

[38] Geidl M, Koeppel G, Favre-Perrod P, Klöckl B, Andersson G, Fröhlich K. Energy hubs for the future. IEEE Power Energy Mag 2007;5:24–30. doi:10.1109/MPAE.2007.264850.

[39] KNMI. North sea climate data. https://www.knmi.nl/nederland-nu/klimatologie/uurgegevens_Noordzee, Accessed: 05.05.2020.

[40] KNMI. Dutch climate data. https://projects.knmi.nl/klimatologie/uurgegevens/selectie.cgi, Accessed: 05.05.2020.

[41] ENTSO-E Transparency Platform. https://transparency.entsoe.eu/, Accessed: 05.05.2020.

[42] CBS. Delivery of electricity for commercial use. https://opendata.cbs.nl/statline/#/CBS/nl/dataset/82538NED/table?ts=1571838451907, Accessed: 05.05.2020.

[43] CBS. Domestic energy consumption by type of household and region. https://opendata.cbs.nl/statline/#/CBS/nl/dataset/81528NED/table?fromstatweb, Accessed: 05.05.2020.

[44] CBS. Composition and size of households by region. https://opendata.cbs.nl/statline/#/CBS/nl/dataset/71486ned/table?ts=1571839741266, Accessed: 05.05.2020.

[45] Gabrielli P, Fürer F, Murray P, Orehounig K, Carmeliet J, Gazzani M, Mazzotti M. A Time-series-based approach for robust design of multi-energy systems with energy storage. Comput Aided Chem Eng 2018;43:525–30. doi:10.1016/B978-0-444-64235-6.50093-0.

[46] Gabrielli P. Optimal Design of Multi-Energy Systems: From Technology Modeling to System Optimization. ETH Zurich; 2019. Ph.D. thesis.

[47] Gabrielli P, Fürer F, Mavromatidis G, Mazzotti M. Robust and optimal design of multi-energy systems with seasonal storage through uncertainty analysis. Appl Energy 2019;238:1192–210. doi:10.1016/j.apenergy.2019.01.064.

[48] McKenna R, Hollnaicher S, Ostman P, Fichtner W. Cost-potentials for large onshore wind turbines in Europe. Energy 2015;83:217–29. doi:10.1016/j.energy.2015.02.016.

[49] The World Bank. Arable land (% of land area). https://data.worldbank.org/indicator/AG.LND.ARBL.ZS?view=chart, Accessed: 25-11-2020.

[50] CBS. Land use. https://opendata.cbs.nl/statline/#/CBS/en/dataset/37105ENG/table?ts=1588690769306, Accessed: 05.05.2020.

[51] The Dutch Ministry of Infrastructure and the Environment. White Paper on Offshore Wind Energy. Tech. Rep.; 2014.

[52] te Raa HR. Bio Jet Fuel from Macro Algae. TU Delft; 2010. Master's thesis.

[53] NREL. Manufacturing Cost Analysis for Proton Exchange Membrane Water Electrolyzers. Tech. Rep.; 2019.

[54] Whiston MM, Azevedo IL, Litster S, Whitefoot KS, Samaras C, Whitacre JF. Expert assessments of the cost and expected future performance of proton exchange membrane fuel cells for vehicles. In: Proceedings of the national academy of sciences of the United States of America; 2019.

[55] IRENA. Renewable Power Generation Costs in 2019. Tech. Rep.; 2020.

[56] Defaix PR, van Sark WGJHM, Worrell E, de Visser E. Technical potential for photovoltaics on buildings in the EU-27. Solar Energy 2012;86:2644–53. doi:10.1016/j.solener.2012.06.007.

[57] Argonne National Laboratory for U.S. Department of Energy. System level analysis of hydrogen storage options. https://www.hydrogen.energy.gov/pdfs/review19/st001_ahluwalia_2019_o.pdf, Accessed: 05.05.2020.

[58] Bloomberg NEF. A behind the scenes take on lithium-ion battery prices. https://about.bnef.com/blog/behind-scenes-take-lithium-ion-battery-prices/, Accessed: 05.05.2020.

[59] CBS. Trends in the Netherlands 2018. https://longreads.cbs.nl/trends18-eng/economy/figures/energy/, Accessed: 26-03-2020.

[60] Jerez S, Thais F, Tobin I, Wild M, Colette A, Yiou P, et al. The CLIMIX model: a tool to create and evaluate spatially-resolved scenarios of photovoltaic and wind power development. Renew Sustain Energy Rev 2015;42:1–15. doi:10.1016/j.rser.2014.09.041.

[61] Markou H, Larsen TJ. Control strategies for operation of pitch regulated turbines above cut-out wind speeds. In: European wind energy conference and exhibition 2009, EWEC 2009; 2009.

[62] MHI Vestas. https://www.mhivestasoffshore.com/mhi-vestas-inks-firm-order-borssele-v-innovation-site/, Accessed: 23-04-2020.

[63] Bauer L., Matysik S.. The big portal for wind energy. www.wind-turbine-models.com, Accessed: 23-04-2020.

[64] The Wind Power. www.thewindpower.net, Accessed: 23-04-2020.

[65] Gemini Wind Park. https://www.geminiwindpark.nl/, Accessed: 26-03-2020.

[66] London Array Wind Park. https://www.4coffshore.com/windfarms/london-array-phase-1-united-kingdom-uk14.html, Accessed: 26-03-2020.

[67] Alam MM, Rehman S, Meyer JP, Al-Hadhrami LM. Review of 600–2500 kW sized wind turbines and optimization of hub height for maximum wind energy yield realization. Renew Sustain Energy Rev 2011;15:3839–49. doi:10.1016/j.rser.2011.07.004.

[68] NREL. Land Use Requirements of Modern Wind Power Plants in the United States. Tech. Rep.; 2009. doi:102172/964608.

[69] CBS. Onshore wind turbines taller and more efficient. https://www.cbs.nl/en-gb/news/2016/39/onshore-wind-turbines-taller-and-more-efficient, Accessed: 09-04-2020.

[70] WindStats. https://windstats.nl/, Accessed: 26-03-2020.

[71] Lloyd SP. Least Squares Quantization in PCM. IEEE Trans Inf Theory 1982;28:129–37. doi:10.1109/TIT.1982.1056489.

[72] Matlab Documentation: kmeans. https://nl.mathworks.com/help/stats/kmeans.html#bvmb8us-1, Accessed: 09-04-2020.

[73] Arthur D, Vassilvitskii S. K-means+ +: the advantages of careful seeding. In: Proceedings of the annual ACM-SIAM symposium on discrete algorithms; 2007.

[74] Kaufman L, Rousseeuw PJ. Finding groups in data: an introduction to cluster analysis. Hoboken, NJ: John Wiley & Sons, Inc; 1990.

[75] IRENA. Renewable Energy Technologies: Cost Anaylsis of Wind Power. Tech. Rep.; 2012.

[76] EWEA. Pure Power: Wind Energy Targets for 2020 and 2030. Tech. Rep.; 2011.

[77] EWEA. The European Offshore Wind Industry Key Trends and Statistics 2010. Tech. Rep.; 2011.

[78] Kikuchi Y, Ishihara T. Upscaling and levelized cost of energy for offshore wind turbines supported by semi-submersible floating platforms. In: Journal of physics: conference series; 2019.

[79] EEA. Europe's Onshore and Offshore Wind Energy Potential: An Assessment of Environmental and Economic Constraints. Tech. Rep.; 2009.

[80] IRENA. Wind costs. http://resourceirena.irena.org/gateway/dashboard/?topic=3&subTopic=31, Accessed: 23-04-2020.

[81] Saadi FH, Lewis NS, McFarland EW. Relative costs of transporting electrical and chemical energy. Energy Environ Sci 2018;11:469–75. doi:10.1039/c7ee01987d.

[82] DNVGL. Filling the data gap: an update of the 2019 hydrogen supply in the Netherlands. https://www.dnvgl.nl/news/filling-the-data-gap-an-update-of-the-2019-hydrogen-supply-in-the-netherlands-162721, Accessed: 08-10-2020.